# STATUS OF THESIS

Title of thesis :

| Development of Multi-Walled Carbon Nanotubes Film for Ionization based Gas Sensing Application |

I, **HENDRAYANA THAHA**

Hereby allow my thesis to be placed at the Information Resource Center (IRC) of Universiti Teknologi PETRONAS (UTP) with the following conditions:

1. The thesis becomes the properties of UTP.

2. The IRC of UTP may make copies of the thesis for academic purposes only.

3. This thesis is classified as
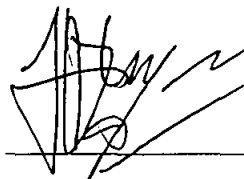
☐ Confidential

[√] Non-confidential

If this thesis is confidential, please state the reason:

_____

_____

The contents of the thesis will remain confidential for ____ years.

Remarks on disclosure:

_____

_____

Endorsed by

_____
Signature of Author

Jl. Saturnus timur 1 no 11, Margahayu
Raya, Bandung, Jawa Barat, Indonesia,
40286

Date : 25 /06 /08

_____
Signature of Supervisor

Name of Supervisor:
Assoc. Prof. Dr. Norani Muti Mohamed

Date : 25 /6 /08

i

# APPROVAL PAGE

UNIVERSITI TEKNOLOGI PETRONAS

Approval by Supervisor (s)

The undersigned certify that they have read, and recommend to The Postgraduate

Studies Programme for acceptance, a thesis entitled "Development of Multi-Walled

Carbon Nanotubes Film for Ionization based Gas Sensing Application" submitted by

**Hendrayana Thaha** for the fulfillment of the requirements for the degree of Master

of Science in Electrical and Electronics Engineering.

25/06/08

Date

Signature          :

Main supervisor    :     Assoc. Prof Dr Norani Muti Mohamed

Date               :     25/6/08

Co-Supervisor      :

Signature          :

Date               :

ii

TITLE PAGE

UNIVERSITI TEKNOLOGI PETRONAS

**Development of Multi-Walled Carbon Nanotubes Film for**

**Ionization based Gas Sensing Application**

By

**Hendrayana Thaha**

A THESIS

SUBMITTED TO THE POSTGRADUATE STUDIES PROGRAMME

AS A REQUIREMENT FOR

THE DEGREE OF MASTER OF SCIENCE

ELECTRICAL AND ELECTRONICS ENGINEERING

BANDAR SERI ISKANDAR,

PERAK

APRIL, 2008

iii

# DECLARATION

I hereby declare that the thesis is based on my original work except for quotations and citations which have been duly acknowledged. I also declare that it has not been previously or concurrently submitted for any other degree at UTP or other institutions.


Signature     :   _____


Name          :   HENDRAYANA THAHA_____


Date          :   _____

# ACKNOWLEDGEMENT

First and foremost, I would like to give my sincere thanks to ALLAH SWT, the almighty God, for giving me the strength, guidance, patience and insight to complete this research.

I am extremely grateful to Assoc. Prof. Dr. Norani Muti Mohamed for giving me a chance to pursue Master degree in Universiti Teknologi Petronas (UTP). She has provided excellent laboratory facilities and patiently gave direction to my finish research in carbon nanotubes for gas sensing application.

It is my pleasure to acknowledge Assoc. Prof. Dr. Bambang Ariwahjoedi for interesting discussion in material science and chemistry. Many thank also to Assoc. Prof. Dr. Sukirno who always supporting for every single step of my study.

I would like to express my gratitude to En Rosli Mohd, the best technologist in UTP, for his assistance, help, and preparing lab facilities during my work in nano lab. My sincere thank also to postgraduate office staffs, Pn Kamaliah, Kak Norma, Kak Haslina and En Fadhil for all assistance during pursuing my master.

I am grateful to postgraduate students, Dani Ihtatho, Kresnajaya Pancakarsa, Firmansyah, Kiki Adi Kurnia, Barkah yusuf widodo, M. Fatiktul Arif, Syauqi, Pak Gunawan, Dedi Atunggal, Bambang Kuncoro, Munir Hidayat, Annisa, Ayu Permana Sari and Pak Totok to keep me mettle while studying in UTP.

A very special mention is due Doctor Chandra Sari for superb long distance health assistance, care, patience, and very deep attention. Finally and the most important, I would like to thank to my family especially to my parents who always give endless supports. Their inexhaustible encourage has been a source of continuous strength all the years.

# ABSTRACT

Nowadays many types of gas sensors have been used to identify and detect the presence of various gases in industrial plants. However, these gas sensors are still facing the problem of lack selectivity and sensitivity for gas detection in ambient temperature and also slow in response time. The objective of this research is to develop multi-walled carbon nanotubes (MWCNTs) film for ionization based gas sensing application. In this study, MWCNTs film is proposed to be used as the active component due to its remarkable electronic and field emission properties for generating ionization mechanism on the gas.

MWCNTs were synthesized by the decomposition of ethylene over metal coated, oxidized silicon substrate in thermal chemical vapor deposition CVD system. Structure and morphology of grown MWCNTs were examined using Raman spectroscopy, scanning electron microscopy (SEM) and transmission electron microscopy (TEM) whilst the electrical properties of nanotubes film were characterized by Van der Pauw and Hall Effect technique. Gas sensing properties testing of MWCNTs film are carried out by identifying gas breakdown voltage between nanotubes film cathode and aluminum film anode. Gasses that have been tested are helium, argon, air, hydrogen 2% in air mixture, and ammonia.

MWCNTs grown using this CVD technique are found to have high crystallinity with typical diameter of 18 nm and length of 1.5 µm. Testing the sensing properties at room temperature reveals that the utilization of MWCNTs film as cathode was able to scale down the air breakdown voltage by a factor of about 58 % as compared to aluminum cathode. On the 10 mL gas volume, helium gas gives the lowest breakdown voltage of about 134 V, whilst air gives the highest value of about 320 V. Further experiment shows that the breakdown voltage is not significantly affected by the gas volume content in testing chamber. Reducing the interelectrode separation by 60 µm results the lowering of the breakdown voltage of helium gas by 122 V. It is concluded that utilization of MWCNTs film as cathode in the ionization based gas sensing configuration is capable to detect helium, argon, air, 2% hydrogen in air mixture, and ammonia at room temperature.

# ABSTRAK

Pada masa kini, terdapat pelbagai jenis sensor gas yang digunakan untuk mengenalpasti dan mengesan kehadiran gas di industri perkilangan. Walau bagaimanapun kebanyakan sensor gas ini masih berhadapan dengan masalah sifat pemilihan dan kepekaan untuk mengesan gas pada suhu persekitaran dengan cepat dan pantas. Objektif penyelidikan ini adalah untuk menghasilkan filem pelbagai-lapisan karbon tiub nano (MWCNTs) untuk ionisasi berdasarkan aplikasi pengesan gas. Dalam kajian ini, filem MWCNTs dicadangkan sebagai komponen aktif oleh kerana ia merupakan komponen elektronik dan mempunyai medan pancaran yang istimewa untuk menghasilkan mekanisma ionisasi kepada gas.

MWCNTs dihasilkan melalui proses pereputan ethelene ke atas lapisan metal, oksida silikon substrat dalam system CVD terma. Struktur dan morfologi pertumbuhan MWCNTs dikaji dengan menggunakan mikroskop Raman, mikroskop elektron imbasan (SEM) dan mikroskop elektron pancaran (TEM) manakala ciri elektrikal filem tiub nano dapat diukur dengan menggunakan teknik Van der Pauw dan Hall Effect. Sifat pengesanan gas filem MWCNTs dilakukan dengan mengesan voltan runtuh antara katoda filem nano tiub dan anod filem aluminum. Gas yang telah diuji setakat ini adalah helium, argon, udara, ammonia, dan 2% Hidrogen dalam udara.

MWCNTs yang dihasilkan daripada teknik CVD didapati mempunyai ciri pengkristalan yang tinggi dengan purata diameter 18 nm dan panjang 1.5 mikron. Uji pengesan gas pada suhu bilik dengan menggunakan filem MWCNTs sebagai katod dapat mengurangkan kadar voltan runtuh sebanyak 58 % berbanding dengan katod Aluminium. Helium pada isipadu 10 mL memberi kesan voltan runtuh yang rendah iaitu lebih kurang 134 V, manakala gas ammonia pula memberi nilai yang paling tinggi iaitu 310 V. Tambahan pula, ujikaji ini membuktikan bahwa voltan runtuh ini tidaklah dipengaruhi oleh isipadu gas pada camber. Pengurangan pemisahan antara eletrod sebanyak 60 mikron menghasilkan pengurangan voltan runtuh gas helium sebanyak 122 V. Secara kesimpulannya, penggunaan filem MWCNTs sebagai katod dalam pengesanan gas secara ionisasi boleh mengesan helium, argon, udara, 2% hidrogen dalam larutan air, dan gas ammonia pada suhu bilik.

# Table of Content

x

j

# List of Tables

# List of Figures

# Chapter 1 : Introduction

## 1.1 Research Background

In view of the rapid growth of industry and transportation using gas as alternative energy source instead of petroleum, the demand of gas sensor as the integrated part of gas appliances increases in recent decades. From the safety point of view, outstanding properties of gas sensor to detect and to identify the presence of gas in environment are critical. Fast response gas sensor property is required in the hazardous environment to trigger early warning system once gas leakage is detected on a system. Highly selective gas detection is one of the important properties of the gas sensor that would prevent miss identification of gas in sensor system which can further lead to system disruption.

Currently, metal oxide based gas sensor is widely used to detect and identify the presence of gas. Unfortunately, this sensor is still encountering drawback such as low selectivity and sensitivity at room temperature operation. Typical metal oxide gas sensors are known to operate at about 300°C to 750°C. High temperature operation will lead to high power consumption. Furthermore the high temperature operation could be hazardous since the sensor may get ignited [1]. The sensitivity of metal oxide based gas sensor has been increased by doping the metal catalyst into sensor active component [1] whereas the selectivity is achieved through gas filtration using the membrane [2].

Rapid technological development of material for electronic, composite, and sensor applications results in the discovery of various materials with remarkable properties. One material which is mostly developed due to extraordinary properties within the two decades is carbon nanotubes. Carbon nanotubes have been developed into many novel electronic devices such as field emitter, transistor, and chemical sensor [3, 4]. Carbon nanotubes has also been used to reinforced polymer composites [5]. Mixture of carbon

1

nanotubes and composites has also been used as the electrode in polymer based super capacitor [6].

One promising applications of carbon nanotubes is as the active component in gas sensing devices. There are several mechanisms used to detect gases using carbon nanotubes. The shifting in resonant frequency of carbon nanotubes resonators as exposed to organic solvent vapors can be used for identifying the gas [7]. The phenomenon of volumetric changing on matrix carbon nanotubes mixed polymer due to gas vapor absorption which lead to percolation of conductivity type has been reported able to detect the presence of gases [8].

Due to the demand of gas sensor in many fields that require high safety standard, sensing properties such as high selectivity and sensitivity, fast response time, and operating at room temperature become of paramount importance to be developed. Carbon nanotube, considered to be $21^{st}$ century material has extraordinary properties believed to give better sensing properties.

## 1.2 Research Objective

Both different types of carbon nanotubes, single walled carbon nanotubes (SWCNTs) and multi-walled carbon nanotubes (MWCNTs) have already been utilized in different sensing applications [9, 10]. However, in order to get highly sensitive carbon nanotubes based sensing device, low defect and highly crystalline CNTs are believed to give better sensing properties.

The objective of this research are:

1. Synthesizing and characterizing carbon nanotubes film for the sensing element in ionization based gas sensor application.

2. Testing gas breakdown voltage over various gases in metal - carbon nanotubes film electrodes

## 1.3 Scopes of Work

The work scopes in this research are divided into following section:

### 1.3.1 Carbon Nanotubes Synthesis

The initial stage of this work is the synthesis of carbon nanotubes which will be used as the active component in gas sensor. The synthesis is carried out using catalytic thermal chemical vapor deposition (CVD) technique. Various metal catalysts layer are used in the growth of carbon nanotubes in order to study the effect of catalyst on the structure and morphology of the nanotubes.

### 1.3.2 Carbon Nanotubes Characterization

The structural characteristic of carbon nanotubes such as defect and crystallinity can be characterized by Raman spectroscopy. Carbon nanotubes film morphology can be analyzed using field emission scanning electron microscopy (SEM) from various angles. The internal structure of carbon nanotubes such as layers and its diameter are obtained through transmission electron microscopy (TEM). Electrical characterization using Van der Pauw and Hall Effect technique give information on the resistivity and charge mobility of carbon nanotubes film respectively.

### 1.3.3 Testing of Carbon Nanotubes as a Gas Sensing Element

Once synthesis and characterization of carbon nanotubes have been carried out, the next stage is the evaluation of carbon nanotubes as the active component for gas sensing application. Testing of the gas sensor is carried out in gas testing chamber which is connected to high voltage power supply to generate electric field in-between electrodes. Voltmeter and ammeter are also connected to power supply to identify gas breakdown voltage on carbon nanotubes – aluminum electrodes. In order to monitor the amount of

gas flow into the testing chamber, gas flow meter and controller module is outfitted in between the gas testing chamber and the gas source. Gases used to investigate the sensing mechanism are oxygen, argon, helium, ammonia, and 2% hydrogen in air mixture.

## 1.4 Thesis Outline

This thesis is organized into five chapters. Chapter 1 elucidates research backgrounds which include recent issue and development in carbon nanotubes based gas sensor applications. The objectives of this research and the scope of work are also outlined within this chapter. The final part of the first chapter describes the layout of the theses.

Chapter 2 reviews current research and development of carbon nanotubes properties, synthesis, analyzing technique, and its application. Field emission from metallic solid state surface, ionization, and gas breakdown voltage in between electrodes literature review is also reviewed within this chapter.

Chapter 3 elucidates research methodology on carbon nanotubes synthesis using catalytic thermal chemical vapor deposition technique. Carbon nanotubes characterization using Raman spectroscopy, SEM, TEM, Van der Pauw, and Hall Effect technique are discussed in detail. This chapter also covers the testing procedure of carbon nanotubes as the active component in the gas sensor.

Chapter 4 discusses the results acquired from this work. The structures of carbon nanotubes will be revealed by Raman spectroscopy whilst nanotubes film morphology will be explained by SEM and TEM analysis. Electrical properties of carbon nanotubes film obtained from Van der Pauw and Hall Effect measurement technique are also explained thoroughly. Discussion on the testing of carbon nanotubes as the sensing component is covered in the last part of this chapter.

Chapter 5 encompasses conclusion of the research along with recommendations for future work.

# Chapter 2 : Literature Reviews

## 2.1 Introduction

Since the discovery of fullerenes in 1985 using vaporization laser technique by Kroto, et al [11] followed by the discovery of carbon nanotubes by Sumio Iljima using arc-discharge evaporator technique [12], both fullerenes and carbon nanotubes have attracted much attention of researcher and industry all over the world due to their remarkable physical, chemical and electronic properties. At present, carbon nanotubes (CNTs) have been used in many novel functional devices [3, 4].

Carbon nanotube can be illustrated as a seamless rolled graphite sheet with closed end cap. Its structure is defined by chiral vector $c$ which pointed the graphite rolled direction as shown in figure 2.1. The chiral vector is shown in equation 2.1

$$c = na_1 + ma_2 \qquad\qquad (2.1)$$

Where:     $a_1$ & $a_2$: unit vectors of graphene in real space.

    n, m  : number of unit vectors
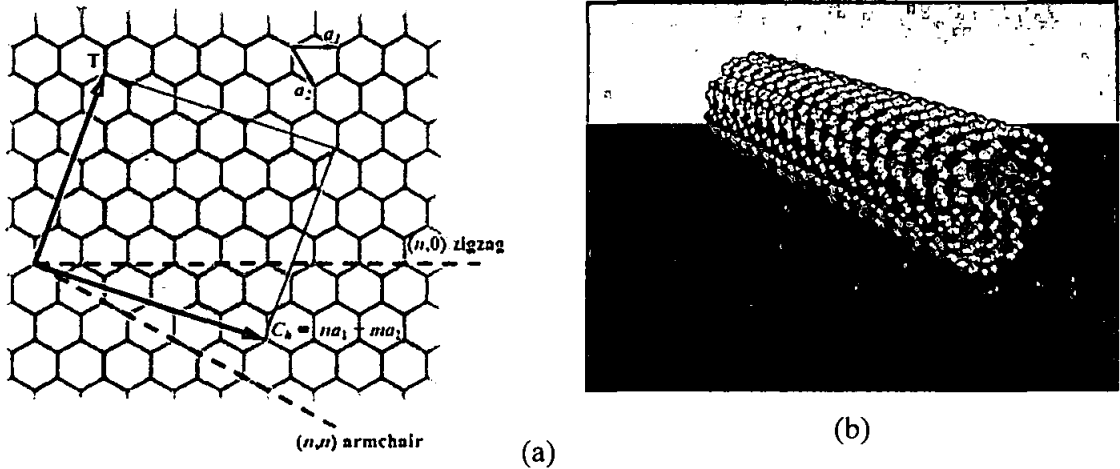


Figure 2-1 (a) Rolled graphite sheets direction [13]. (b) Single-walled carbon nanotubes [14].

Carbon nanotubes chiral angle is determined by its chiral vector. Chiral vector angle to base vector $a_1$ is shown in equation 2.2.

$$\cos\theta = \frac{n + m/2}{\sqrt{n^2 + nm + m^2}}$$ (2.2)

Where:     $\theta$     : carbon nanotubes chiral angle

           n, m   : number of unit vectors

Carbon nanotubes diameter is given by the chiral vector length in circumference as shown in equation 2.3.

$$d = \frac{|c|}{\pi} = \frac{a_0\sqrt{n^2 + nm + m^2}}{\pi}$$ (2.3)

Where:     $d$     : carbon nanotubes diameter

           $a_0$   : 0.1424 nm

The smallest graphene lattice vector perpendicular to chiral vector defines the translational period ($T$) along tube axis. The equation 2.3 shows the translational vector in nanotubes. The $\chi$ in equation 2.4 is greatest common divisor of (m, n) whereas $\Re$ =3 if [(n-m) / (3)] is integer and $\Re$ = 1 otherwise.

$$T = -\frac{2m + n}{\chi\Re}a_1 + \frac{2n + m}{\chi\Re}a_2$$ (2,4)

The nanotubes with m = 0 is called zigzag nanotubes since this chiral vector will give zigzag pattern along the circumference. Nanotubes with n = m is armchair nanotubes [15].

Carbon nanotubes can be classified into two type's namely multi-walled carbon nanotubes (MWCNTs) and single walled carbon nanotubes (SWCNTs). MWCNT is formed by individual layers making up the concentric tubes. MWCNTs cap contain pentagonal carbon rings but sometimes in practice complex cup structure is observed such as heptagonal carbon rings. The appearance of SWCNTs as shown in figure 2.1(b) is

quite different to MWCNTs since SWCNTs only have single rolled graphite sheet and have small diameter (typically~1nm) [16].

## 2.2 Carbon Nanotubes Properties

### 2.2.1 Electronic Properties

Carbon nanotubes electronic properties can either be semiconducting or metallic. The nanotubes chiral vector determines its properties. Carbon nanotubes is metallic as the vector unit value on chiral vector equal to n–m = $3i$ ($i$ is integer). If the vector unit value n–m $\neq$ $3i$ ($i$ is integer), the nanotubes electronic properties is semiconducting.

SWCNTs have remarkable properties and have been implemented in many electronic applications. One of its superior properties is the electrical transport which is reported to be up to $10^9 A/cm^2$ [17]. High electrical transport property is very suitable for superconductor application.

Resistivity measurement on bundle MWCNTs of ~210 μm in length and ~15 nm in diameter result in 0.009 $\Omega$ cm [18]. The resistivity of carbon nanotubes is influenced by its substrate. Growing MWCNTs over $Al_2O_3$ as substrate resulted in higher resistivity of nanotubes compared to growing over silicon dioxide substrate. The reason behind this peculiar property is the roughness of $Al_2O_3$ surface which is higher than $SiO_2$ surface [19]. Since the resistivity of MWCNTs is affected by the defect, resistivity measurement of CNT can be used for knowing the carbon nanotubes crystallites [20]

### 2.2.2 Field Emission Properties

Carbon nanotubes have been utilized for field emission device applications. This application is highly influenced by electronic properties at the nanotubes tips since the open ended SWCNTs work function on the tips is lower than closed ended SWNT [21].

The simulation using average current density with simplified Fowler Nordheim formula shows that the field emission properties of carbon nanotubes array is influenced by its array density and its height [22]. Self-assembly structure of carbon nanotubes technique had been developed to be implemented on field emission application based nanotubes. The enhancement of emission site and more uniform emission can be achieved by post treatment to the sample using ethanol. This suggests that the treatment affects the surface morphology of the sample [23]. The synthesis and catalyst also affect the field emission properties since different synthesis process yields different characteristics of nanotubes [24].

### 2.2.3 Mechanical Properties

Carbon nanotubes have been used to reinforce the composite material because of their extraordinary mechanical properties. Simulation using MWCNTs model as individual nested SWCNTs layer with Van der Waals force in between the layer results average modulus young of $1.05 \pm 0.05$ Terra Pascal and shear moduli of $0.4 \pm 0.05$ Terra Pascal. The simulation shows that both Young modulus and shear moduli are affected by nanotubes chirality and number of walls on MWCNTs. Young Modulus increase as the number of walls increases. The different number of layer gives different Young modulus. As obtained form simulation, zigzag nanotube gives higher Young modulus than arm chair nanotubes with the same wall number. Shear moduli obtained is 0.4 Terra Pascal. Furthermore, nanotubes shear moduli decreases as the nanotube diameter increases. It was found that the effect of tube chirality to shear moduli is not significant. For both zigzag and armchair MWCNTs, the shear moduli are reduces as the number of tube layers increases [25].

### 2.3 Growth Mechanism of Carbon Nanotubes

Solid liquid solid model is suggested by Gorbunov et al (2002) to describe carbon nanotubes growth mechanism. The metal catalyst acts as the medium for growing nanostructure in this model. The supersaturated decomposed atom carbon is precipitated

through molten catalytic particle to form tubular structure [26]. In addition, the size of catalyst particles affects the yield of carbon nanotubes. The diffusion of carbon atom on big catalyst particle is not efficient hence results in low yield of carbon nanotubes [27]. The atom carbon diffuses along the metal catalyst and precipitates on the opposite half, around, and below the bisecting diameter to form nanotubes wall. Since the atom carbon does not precipitate from the apex of the catalyst hemisphere, the carbon atoms create the hollow core with the circumference of seamless graphite sheet [28].

Typically the growth type of carbon nanotubes can be classified into two type namely base growth and tip growth. On the base growth type, the carbon atoms extrude through the metal catalyst hence which then creating nanotube wall. The metal catalyst remain attached to the substrate on the base type growth whist the particle detach and move at the tips of the growing nanotubes on tip growth type [28]. Schematically the growth mechanism is shown in figure 2.2.
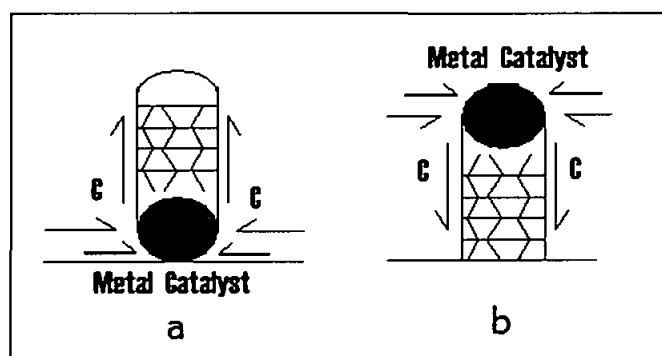
Figure 2-2 Growth type of carbon nanotubes. (a) Base growth, (b) Tip growth.

## 2.4 Synthesizing Technique for Producing Carbon Nanotubes

Four main techniques commonly used for synthesizing carbon nanotubes are arc discharge, laser ablation, plasma enhancement chemical vapor deposition (PECVD), and thermal chemical vapor deposition (CVD). Detail explanations of synthesizing technique on thermal CVD technique will be given whilst other techniques are explained briefly.

### 2.3.1 Arc Discharge

Carbon nanotube was first obtained from arc discharge technique [12]. The method arc evaporation of two graphite rod electrodes with separation of about 1 mm is carried out by creating plasma in the electrode. The outcomes of this synthesis technique are in carbon nanotubes bulk form.

The structure of carbon nanotubes produced using arc discharge technique is influenced by synthesis pressure, gas atmosphere, electrode type, voltage, and current on graphite electrode. To obtain high quality single walled carbon nanotubes using arc discharge technique, nickel and yttrium compound are utilized as catalyst in graphite electrode. The synthesis is carried out in helium atmosphere at 530-550 Torr in pressure [29]. Carbon nanotubes synthesis using DC arc discharge utilizing pure graphite electrode can also be carried out in dry air atmosphere. The nanotubes synthesized in air atmosphere have a great reduction in carbon soot compared to the ones synthesized in helium atmosphere. The optimum pressure to produce high yield multiwalled carbon nanotubes using this technique is 300 Torr [30].

### 2.3.2 Laser Ablation

Another synthesis technique to produce carbon nanotubes in bulk form is through laser ablation. The nanotubes are obtained through graphite evaporation assisted by laser which can be carried out in either high temperature or in room temperature reactor. In addition, either continues or pulse laser can be used in this technique.

In order to obtain high yield SWCNTs, compressed graphite mixture of nickel and cobalt catalyst with addition of either nitrates or acetates is used as targeted material. The synthesis is carried out in 1 bar of pressure in nitrogen atmosphere. A pulse energy of

2.5GW Q-switched Nd:YAG laser with wavelength of 1.064 nm and frequency of 10 Hz is used to decompose carbon in targeted material [31]. Multiwalled carbon nanotubes can be obtained by laser ablation technique at room temperature using 248 nm KrF laser. This technique is performed in oxygen atmosphere pressure of 2 Torr. Both Ni-doped and Ni–Co doped graphite is utilized as carbon source in this technique. The yield of this ablation technique is carbon nanotubes with diameters of 100 nm to 200 nm and length of 1.0 mm to 3.5 mm [32].

### 2.3.3  Plasma Enhancement Chemical Vapor Deposition

Carbon nanotubes synthesis can be carried using plasma enhancement CVD (PECVD) technique. Both nickel and cobalt ultra thin films were be utilized as catalyst in this technique [33]. Either ethylene or methane can be used as the carbon feedstock on carbon molecule decomposition over the catalyst film. For the hot filament PECVD that used methane, ammonia was added during the process of growing nanotubes in order to improve the diffusion of carbon atom in catalyst particles [34]. The synthesis temperature influences the nanotubes diameter in such a way that higher temperature leads to increase the diameter [35].

### 2.3.4  Thermal Chemical Vapor Deposition

Thermal CVD technique is able to synthesis carbon nanotubes. One advantage using this technique is that the row product already in film form hence no further processing is required to form nanotubes in film. In addition, no purification subjected to nanotubes film after the synthesis since very low amorphous carbon formed over the film. Thermal CVD reactor, substrate preparation, and synthesizing process would be described in detail in the following subsection

### 2.3.4.1 Thermal CVD Reactor

Heating technique for thermal CVD can either be cold wall or hot wall reactor. On cold wall CVD reactor, substrate is heated directly by either induction heating or radiant heating while the rest of reactor remains cool. On hot wall CVD reactor the substrate is placed on isothermal furnace.

Carbon nanotubes synthesis can be carried out in cold wall CVD reactor. The substrate is heated directly and uniformly in this reactor system. Heater is placed below the substrate causing the heating to take place only on the substrate. The distance between substrate and gas source outlet is about 2 cm. Carbon feedstock for synthesizing nanotubes using this method is methane. Hydrogen is flown into the system while synthesizing taking place. All gasses which involve during nanotubes synthesis are controlled by using gas flow controller. The pressure in cold wall CVD chamber is kept constant while synthesizing nanotubes [36].

Hot wall CVD can also be used for synthesizing carbon nanotubes. Typical hot wall thermal CVD is shown in figure 2.3. The schematic shows that heating process induced to all furnace tubes. Since higher yield CNT can be produced by thermal CVD technique, this technique becomes one of the most promising techniques in term of large industrial scale.
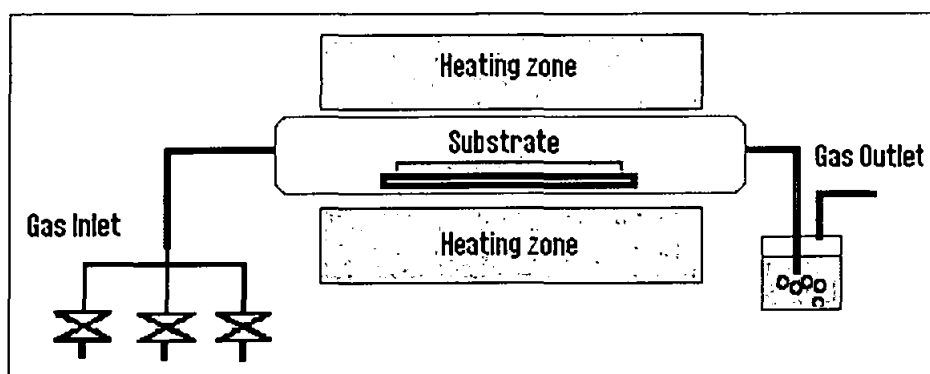


Figure 2-3 Typical thermal CVD reactor.

### 2.3.4.2 Sample Preparation

Catalyst particles are required in carbon nanotubes synthesis. Catalyst can be deposited onto substrate using sputtering machine, spin coater, electron beam evaporator, sol gel, and thermophoresis apparatus. Either single transition metal catalyst or mixtures from several metals can be deposited using those equipments. The thickness of nano film catalyst is controlled by the deposition parameter of the respective equipments.

Sputtering technique is able to deposit metal catalyst directly onto the substrate. Not only single metal catalyst but also mixed metal catalyst with another chemical element, such as molybdenum, can be deposited using this technique. Two sputtering techniques can be used to deposit catalyst particle, namely multilayer sputtering and co-sputtering techniques. In the first technique, nano metal catalyst particle and other chemical element are deposited layer by layer over the substrate prior to nanotubes synthesis in CVD system. In the second method, metal catalyst is mixed with another chemical element prior to the deposition process onto the substrate. Well dispersed mixture in the second method gives better uniformity of nanotubes yield compared to the first method [37].

Spin coating technique can be utilized to deposit metal catalyst film onto the substrate. Nano particle catalyst is first diluted in toluene solution before the coating process on the substrate by spin coater. The concentration of nano particle catalyst in dispersed solution will affect the yield of CNTs [38]

Nano particle catalyst can also be deposited by using electron beam evaporator. In order to avoid interaction between silicon wafer and catalyst layer, catalyst buffer layer is formed on the substrate. The buffer layer, such as $Al_2O_3$, and metal catalyst particle can be deposited using the same equipment [39]. The experiment shows that $Al_2O_3$ buffer layer gives more defective nanotubes compare to nanotubes grown over $SiO_2$ buffer layer [19].

Sol gel technique can be used for depositing metal catalyst particle onto $Al_2O_3$ layer. The metal catalyst is prepared from different metal precursor, specifically $Fe(NO_3)_3$, $Fe(acac)_3$, $Co(OAc)_2$, and $Co(acac)_2$. Bimetal catalyst particle can be formed either from the mixture of $Fe(NO_3)_3$ and $Co(OAc)_2$ or mixture of $Fe(acac)_3$ and $Co(acac)_2$. Ethylene gas is used as carbon feedstock in growing CNT using this technique. This technique had shown that the metal precursor $Fe(NO_3)_3$ gives better activity compare to $Fe(acac)_3$ [40].

Another technique to deposit iron catalyst onto $SiO_2$ substrate is thermophoresis. In this technique, iron catalyst is deposited by using hot wire generator (HWG). The catalyst deposition process can be carried out either as ex situ process where HWG is separated from precipitator or as in situ process. The particle size is affected by HWG temperature, flow rate and separation between HWG and thermophoretic precipitator. Iron catalyst on substrate is subjected to reduction process by flowing in $H_2/N_2$ gas for 5 minute. The carbon feedstock for growing CNT in this method is CO gas. The catalyst deposition by using ex situ HWG proven to produce double walled carbon nanotubes whilst in situ HWG process, SWNT is produced instead [41].

Transition metal such as nickel, cobalt, and iron can be used as catalyst in synthesizing carbon nanotubes by using thermal CVD technique. Molybdenum can also be added into the catalyst in order to produce high yield nanotubes. Catalyst option is depending on the carbon feedstock and temperature while growing CNT.

Nickel can be used as catalyst in the synthesis of carbon nanotubes. Electron beam evaporator has the capability to deposit nickel catalyst onto substrate with the thickness variation of 1 nm to 50 nm. This technique utilized methane as carbon feedstock for growing nanotubes. Prior to synthesis process, the catalyzed coated substrate is soaked in nitrogen atmosphere at 740°C for 15 minutes. For thick catalyst film of 50 nm, the catalyst formation island is not happening hence no carbon nanotubes are synthesized. Formation of carbon nanotubes can only be observed at temperature below 700°C [42].

Instead of nickel, iron can also be used as catalyst in synthesizing carbon nanotubes. Metal vapor vacuum arc with adjustable deposition angle can be used to deposit iron catalyst onto the substrate. Nanotubes synthesis is started by flowing in hydrogen for one hour in 580°C prior to carbon decomposition. Temperature is elevated until it reached the growing temperature in hydrogen atmosphere. Acetylene and hydrogen gas is flown over the substrate during nanotubes growing process. The result showed that the deposition angle catalyst determines the catalyst particle size which further affect nanotubes diameter [43].

Another catalyst that can be used to grow carbon nanotubes is cobalt. Cobalt deposition can be carried out by using spin coating technique. Higher molar catalyst solution creates higher particle density over $SiO_2$ substrate. The high density catalysts over the substrate produce well aligned CNT. The carbon feedstock for this process is acetylene with the synthesis temperature of 850°C [44].

Mixtures of two transition metals have been used for catalyst instead of single metal catalyst. Bimetal catalyst in non oxidative atmosphere is prepared by impregnation of nickel and iron nitrate. Catalyst reduction process is carried out in hydrogen atmosphere for 6 hours at 600°C prior to nanotubes synthesis. In non oxidative environment, mixture of two metals as catalyst was found to increase the catalyst activity. Nickel catalyst activity can be suppressed when mixture of nickel and iron catalyst being used in growing CNT in oxidative environment [45]. In addition carbon nanotubes can also be grown over bimetal cobalt iron catalyst coated substrate. The carbon decomposition process is carried out at temperature in the range of 823 to 1023 K with ethylene gas as carbon feedstock. The main product from ethylene decomposition over $Al_2O_3$ supported catalyst is MWCNTs. Without $Al_2O_3$ supporting layer, graphite crystal is formed [46].

Catalyst thickness plays an important role in carbon nanotubes synthesis. The catalyst thickness has to proper with nanotubes growing parameter and growing technique. The carbon nanotubes are only produced if acetylene is able to diffuse into catalyst cluster. Higher temperature results longer diffusion length inside catalyst cluster. Therefore

thicker catalyst cluster requires higher temperature for growing carbon nanotubes using thermal CVD method [47].

## 2.3.4.3    Synthesizing Process

Several gases can be utilized as carbon feedstock in carbon nanotubes synthesis namely methane, ethylene, acetylene, and carbon monoxide. In addition, ethanol vapor can also be used as carbon feedstock for growing nanotubes over nano metal catalyst substrate.

Methane gas can be used as carbon feedstock in carbon nanotubes synthesis using nickel particle catalyst. The respective carbon feedstock and catalyst composition produce carbon nanotubes either with bamboo defect or nanofiber form. Nanotubes produced using this technique is affected mainly by the growing temperature [48]. Growing nanotubes using methane as carbon feedstock can also produce "Y" type junction nanotubes. The "Y" junction nanotubes are formed on NiO-CuO-MoO coated silicon oxide substrate with methane decomposition at 700°C in atmospheric pressure [49]. MWCNTs have also been reported to be produced by methane decomposition over $CuSO_4$ coated $Al_2O_3$ substrate [50].

Acetylene gas can be utilized as carbon precursor for nanotubes growing process over cobalt catalyst on MgO powder. Carbon decomposition over cobalt supported MgO at 600°C results in MWCNTs. The percentage of cobalt in MgO mixture affects both yield and quality of nanotubes. Loading 50% cobalt into MgO gives optimum yield of carbon nanotubes whilst loading 25% cobalt results in high quality carbon nanotubes [51].

Ethylene gas can be used as carbon feedstock in synthesizing carbon nanotubes. The synthesis is carried out in atmospheric pressure with temperature of 600°C. Combination ethylene and cyclopentadienly iron lead to MWCNT with typical diameter of 40 nm to 80 nm [52].

Ethanol is one of the carbon precursors which can be used for synthesizing nanotubes over cobalt and iron coated conducting glass, quartz or porous alumina substrate. Ethanol decomposition at 700°C over nickel plate has been found to produce carbon nanotubes. The yield of carbon nanotubes was found to be affected by supported substrate catalyst. Ethanol decomposition over conducting glass produces MWCNTs whilst curled SWCNTs would be obtained if nickel plate is used as substrate. Moreover, Cervanteza (2005) had discovered the nanotubes diameter grown over porous alumina is smaller than the ones on nickel plate [53]. Ethanol decomposition over 5 nm iron catalyst coated quartz at atmospheric pressure and oxidizing atmosphere of 850°C yields MWCNTs [54].

Temperature and pressure during the synthesis of carbon nanotubes are two factors that can affect the yield. Variation of temperature and pressure during the synthesis of carbon nanotubes lead to different structure and nanotubes types.

One of the potential applications of carbon nanotubes is field emission display (FED). This application requires hollow carbon nanotubes rather than bamboo shaped nanotubes. Decomposition of acetylene gas over nickel catalyst at 550°C for 10 minutes results in hollow nanotubes. The use of lower pressure lower than the atmospheric pressure increases the nanotube growth rate [55].

Carbon nanotubes synthesis can be carried out at the pressure of 90 Torr. Ethylene is flown over nickel catalyst coated substrate for 20 minutes. This technique resulted in well aligned nanotubes at 400°C growing process. Higher temperature i.e. 500°C and 600°C produced poor alignment with higher growth rate [56].

Synthesis of carbon nanotubes over iron catalyst coated $Si/SiO_2$ substrate can be carried out in CVD rapid heating and cooling system. The synthesis is carried out at 10 Torr pressure with acetylene as carbon feedstock and the growth temperature range of 700°C to 900°C. In this technique cooling process to 250°C takes less than 25 seconds. The nanotubes growth rate over $SiO_2$ was found to increase if the temperature increases. Thicker deposited catalyst was found to give larger diameter nanotubes [57].

Carbon nanotubes can be synthesized at 350°C and 500°C using cold wall CVD system. Iron and aluminum/iron/aluminum (Al/Fe/Al) thin film can be used as the catalyst. It was found that Al/Fe/Al thin catalyst film layer produce high yield nanotubes compared to iron catalyst film. Annealing process in $NH_3$ atmosphere was carried out prior to growing nanotubes on acetylene atmosphere. At the growth temperature of 500°C narrower diameter distribution was obtained compared to the one growing at 350°C. Moreover, nanotubes defect was found to be lower when the nanotube synthesis was carried out at 500°C [58].

## 2.5 Carbon Nanotubes Film Characterization Technique

### 2.5.1 Raman Spectroscopy

Raman Spectroscopy was founded by Sir Chandrasekhar Venkata Raman in 1928. At the early stage of spectroscopy development, sunlight collected by telescope was used as light source. Various lamp developments have been taken into account in order to achieve better excitation source. Mercury lamp was practically used for excitation source. Nowadays lasers with variety of wavelength such as Ar+ (351 nm - 514.5 nm) and YAG (1.064 nm) are available for Raman spectroscopy. Starting with detection of Raman spectra with naked eye by the inventor, the detector gradually improved to detect more sensitive Raman scattering. The detection techniques continuously developed starting with the use of photographic plate to photo electronic [59].

In order to find out its Raman spectra, the material should be irradiated by high intensity laser. The scattered light from sample consist of two components namely Rayleigh scattering and Raman scattering. The photon frequency of laser remains the same in Rayleigh scattering since there is no photon frequency shifting before and after collision with the electron on sample. The photon frequency shifting merely occurs when Raman scattering is involved. The scattering frequency of photon is equivalent to the vibrational frequency of the molecules in the sample [59]. The displacements of the carbon atoms in

radial direction which occur around 165 cm$^{-1}$ is calculated as radial breathing mode (RBM). Cyclic boundary condition on rolled graphite sheet into tube causes degeneration in CNT. The degeneration of tangential mode in nanotubes Raman scattering is represented by two peaks around 1582 cm$^{-1}$. Disordered band (D-Band) on SWCNTs Raman spectra is observed around 1300 cm$^{-1}$. D-Band mode is similar with vibrational mode seen in graphite in term of its position and dispersive mature [60]. Hence, Raman spectrum analysis with the frequency shift in the of range 100 to 1800 cm$^{-1}$ can be used to determine nanotubes structure through RBM, D-Band and graphitic band (G-band) analysis.

One of the distinctive properties of SWCNTs is the coherent vibration occurring in radial direction known as radial breathing mode (RBM) with the presence of splitting peak in G-band region. The information of RBM frequency can be used to extract diameter and chirality of CNT [61]. The RBM peaks can occur in several frequency numbers in one spot observation. Raman spectra with sufficient intensity can be observed as the separation energy $E_{ii}$ and Van Hove singularities is very close to laser excitation energy. The observed SWNT must have energy $E_{ii}$ in the range of ± 0.10 eV. In nanotubes Raman experiment, armchair, and chiral nanotubes have biggest probability to give highest signal within resonant energy window [62].

Structure and diameter characterization of isolated SWNT can be carried out using resonant confocal micro Raman spectroscopy within frequency range of 100 cm$^{-1}$ to 1800 cm$^{-1}$. SWCNTs diameter ($d_t$) can be resolved using inverse proportional relationship Raman shift frequency to SWNT diameter, accordingly to equation 2.4.

$$\omega_{RBM} = 248/d_t \qquad (2.5)$$

Where:     $\omega_{RBM}$: Radial breathing mode frequency

$d_t$: Single walled carbon nanotubes diameter

SWCNTs structural assignment can be ascertained by identifying laser excitation energy resonance with the nanotubes. A nanotube is predicted to be in resonance with laser within the range of ± 0.1 eV. Nanotubes with specific structure would have high resonance possibilities to be selected. SWNT with big chiral angle have higher probabilities to give higher Raman intensities [62].

Diameter assignment on bundle SWNT can also be determined using Raman spectroscopy. Since inter-tubes interactions affect SWNT electronic density of state, the correlation between Raman frequencies shifting on bundle SWNT is shown in equation 2.5 [63].

$$\omega_{RBM} = \frac{244cm^{-1}}{d_t} + 14cm^{-1}$$ (2.6)

Where:                    $\omega_{RBM}$: Radial breathing mode frequency

$d_t$: Single walled carbon nanotubes diameter

The D-band occurring in the first order Raman spectra is due to a defect induced on carbon nanotubes. D-band peak in spectra occurs around 1350 cm$^{-1}$. The peak position is affected by laser excitation energy given to the sample. The energy shift of the main peak increases with decreasing tube diameter [64]. The graphitic band (G-Band) is observed within the range of 1500 to 1600 cm$^{-1}$ in Raman spectra. The shape and intensity of this mode is also affected by laser excitation energy [65].

Raman spectroscopy can also be used to characterize the structure of MWCNTs. Zhang (2001) found that on highly crystalline MWCNTs, the ratio of D-Band to G-Band ($I_d/I_g$) is less than one [66]. Furthermore Singjai (2007) reported that Raman spectroscopy can be utilized to determine MWCNTs on bulk form qualitatively. The higher value of ($I_d/I_g$) ratio leads to higher conductivity of the bulk nanotubes [20].

### 2.5.2  Scanning Electron Microscopy

Since human eyes ability to observe an object is limited beyond the resolution of about 100 μm, an additional device is required to study micro and nano structure. Scanning electron microscopy is a magnification tools which uses electron beam instead of visible light to reveal micro or nano structure.

The electrons source is focused into a fine probe that is rastered over the surface of the specimen in vacuum chamber. As the electrons penetrate the surface, a number of interactions occur that result in the emission of electrons or photons either from or through the surface. A reasonable fraction of the electrons emitted from specimen collected by detectors can be used to modulate the brightness image of sample shown in display screen [67].

Field emission scanning electron microscopy (FESEM) is another type of SEM that can be used for studying nano material structure. One of the advantages of using FESEM is that the observation result is acquired faster compared to scanning probe microscopy (SPM). Nanotubes observation using FESEM shows that differences in surface electrostatic potential are responsible for the contrast between the nanotubes and substrate observed. Increasing magnification, or increasing beam current are found to reduce the image contrast [68].

### 2.5.3  Transmission Electron Microscopy

Transmission electron microscopy can be utilized to observe micro and nano structure due to its very high image resolution. On some high voltage TEM instrument the resolution higher than 0.2 nm can be acquired. Image captured by TEM is obtained from both undeflected and deflected electron that penetrate thin sample (less than 200 nm). A series of magnetic lenses over and below the sample position are responsible for delivering the signal to a detector. A fluorescent screen, a film plate, or a video camera usually used as a detector. TEM offers two methods of specimen observation, diffraction

mode and image mode. In diffraction mode, an electron diffraction pattern is obtained on the fluorescent screen whilst the image mode produces an image of the illuminated sample area. The image can contain contrast brought about by several mechanisms: mass contrast, due to spatial separations between distinct atomic constituents; thickness contrast, due to non uniformity in sample thickness; diffraction contrast, which in the case of crystalline materials results from scattering of the incident electron wave by structural defects; and phase contrast [67].

Due to the capability of acquiring nano scale high resolution picture, the TEM is widely used to characterize the internal structure of carbon nanotubes such as internal diameter, growth type and defect on nanotubes wall. In addition, TEM is preferred to be used as one of various characterization techniques because of simple preparation and the characterization will not make any damage to the nanotubes structure.

### 2.5.4 Van Der Pauw Thin Film Resistivity Measurement

Since film thickness affects the film resistivity and also current flow laterally on thin layer, sheet resistance (ohm/square) is used for measuring resistance in thin film. A method to measure sheet resistivity is by using Van der Pauw method. One of the advantages of using Van der Pauw method is the sheet resistivity measurement that can be carried for irregular shape sample. The sheet resistance $R_s$ measurement is given by equation 2.6.

$$R_s = \left( \frac{\pi d}{\ln 2} \right) \left( \frac{Ra + Rb}{2} \right) f\left( \frac{Ra}{Rb} \right) \tag{2.7}$$

Where:         $R_a = V_{34}/I_{12}$ and $R_b = V_{14}/I_{23}$.

Van der pauw function $f(R_a/R_b)$ is equal to one as the contact placed symmetrically about a line through any pair of nonadjacent contact [69]. Van der Pauw schematic diagram is shown in figure 2.4.
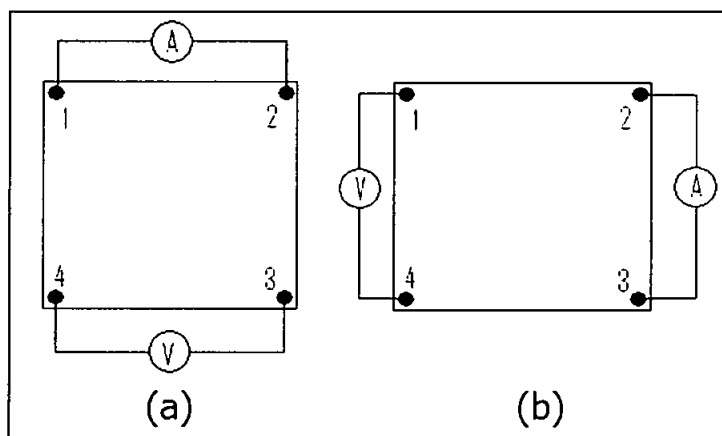


Figure 2-4 Van der Pauw technique for thin film resistivity measurement (a) horizontal resistivity measurement (b) vertical resistivity measurement.

Lia et al (2002) reported sheet resistivity measurement using on well oriented carbon nanotubes continuous ribbon results in $12.6 \times 10^{-4} \ \Omega cm^{-2}$ [70].

## 2.5.5    Hall Effect on The Sample

Hall Effect was discovered by Edwin Hall in 1897. The effect occurs when the magnetic field is applied perpendicular to the electron flow on conductance sheet as shown in figure 2.5. Due to Lorenz force experienced by charge, the electrons accumulate on a side of conductance sheet. Since the conductance sheet is neutral before, then some positive ion at another side will be deprived of their compensating electron. The polarity on the sheet results in internal electric field between two sheet sides [71].
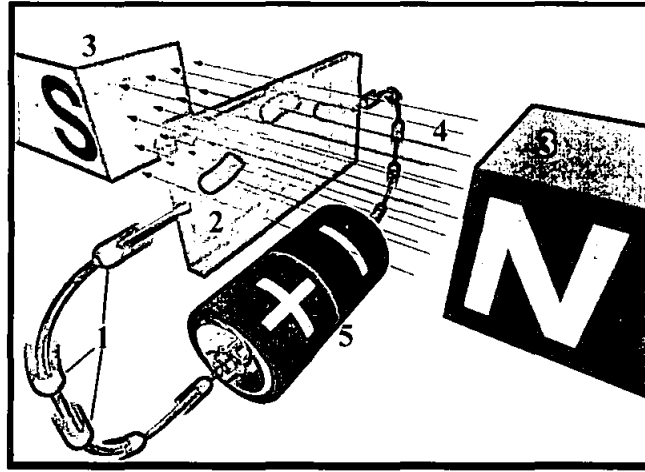
Figure 2-5 Hall Effect schematic: (1) electron, (2) thin film, (3) Magnet, (4) Magnetic field, (5) power supply [72].

The internal electric field in correlation with Hall coefficient , current density and magnetic field $(B)$ are shown in equation whilst the electron density correlation to hall coefficient are shown in equation (2.7) and (2.8) respectively [71].

$$\varepsilon_H = R_H J B \qquad\qquad (2.8)$$

$$R_H = \frac{1}{N_e e} \qquad\qquad (2.9)$$

Where:      $\varepsilon_H$ : Internal electric field      $R_H$ : Hall coefficient

J : Current Density      B: Magnetic field

$N_e$: Charge carrier density

**2.6 Carbon Nanotubes Application**

**2.6.1   Field Emission Display**

One of the potential applications of nanotubes based devices is field emission display (FED) fabricated by using nanotube organic binders. The paste of well dispersed carbon nanotubes is squeezed onto the metal patterned sodalime glass through the metal mesh of 20 μm in size and subsequently heat treated in order to remove the organic binder. Phosphor coated glass is placed over dispersed nanotubes with spacer thicknesses of 200 μm. Choi et al (1999) reported that the turn-on field of FED less than 1 V/mm and emission currents of 1.5 mA at 3 V/mm with current density $J$ 590 mA/cm$^2$ were achieved using this technique. Further observation results in the brightness of 1800 cd/m$^2$ at 3.7 V/mm [73].

**2.6.2   Solar Cell**

Carbon nanotubes can be used to improve conversion efficiency in dye sensitized solar cells (DSCs). Purified nanotubes mixed with sol gel solution, which formed from mixture of isoperoxide, isopropanol, nitride acid, and distilled water, followed by drying in 80°C for one hour to get $TiO_2$-CNT filtrate. Nanotubes coating over $TiO_2$ improve conversion efficiency value around 50% in DSCs [74].

**2.6.3   Super Capacitor**

Another interesting application of carbon nanotubes is high capacitance electronic device for energy storage. Mixing purified carbon nanotubes with phenolic resin powder followed by molding process for 15 minutes in 100°C is the first stage of obtaining high capacitance capacitor. The processing then continued with carbonization process of sample at 850°C. Chemical treatment using nitride acid and sulfuric acid subjected to the sample was found to increase the capacitance of $H_2SO_4$ electrolyte based capacitor [75].

### 2.6.4 Molecular Transistor

Since carbon nanotubes represent new building blocks in nanotechnology, many application based on nanotubes have been made using nano manipulation devices. AFM can be utilized to make field effect transistor using single SWCNTs. The AFM tip with very low force, 10-50 nN, is employed to interpose the nanotubes in Au electrode [76]. Dielectrophoresis is another technique to make carbon nanotubes field emission transistor. In order to connect nanotubes between electrodes on substrates, purified nanotubes are suspended using isopropyl alcohol (IPA) followed by dropping nanotubes suspension and subjected to frequency 10 MHz AC bias. The number of nanotubes connects two electrode is affected by dielectrophoresis deposition time, longer deposition time results more nanotubes connected in between two electrodes [77].

MWCNT can also be used as single electron transistor instead SWCNT. The carbon nanotube is positioned on top of two 20-nm thick gold leads using AFM manipulation. Contact resistance of 10–20 kV is obtained from heat treatment at 1000 K for 10 - 30 s after manipulation using AFM. The measured equivalent background charge noise is in the range $2 \times 10^{-5} - 6 \times 10^{-6}$ /Hz $^{1/2}$ at frequencies of 10 – 45 Hz [78].

### 2.7 Gas Sensor Based Carbon Nanotubes

Carbon nanotubes can be used as active sensing element in either chemical or physical sensor application [79]. The frequency shifting of nanotubes resonator can be utilized to detect the presence of gas in a system. One of mostly used techniques is the measurement of resistivity or conductance over gas exposure to nanotubes film. The other technique is through gas finger print obtained from breakdown voltage in nanotubes electrode. The nanotubes based gas sensing method will be explained in detail in following section.

### 2.7.1 Carbon Nanotubes Resonators

Since resonant frequency of a resonator depends on the dielectric constant of the material, the shifting frequency of disk resonator due to dielectric changing can be employed for sensing application. Carbon nanotubes can be utilized to improve sensitivity on micro strip circular disk resonator. Circular disk resonator coated with carbon nanotubes 0.5 mm in thickness results frequency shifting once exposed to ammonia whilst uncoated disk gives no frequency shifting. The shifting is attributed by the changes on effective dielectric constant on carbon nanotubes coated substrate since ammonia interacts with carbon nanotubes wall. Single walled carbon nanotube was found to give more sensitive response compared to multi walled carbon nanotubes disk resonator [80].

### 2.7.2 Resistivity Variation

One of implemented technique for gas identification is by detection of resistance variation due to gas exposure to nanotubes film. This technique was applied using MWCNTs film grown over cobalt catalyst through thermal CVD technique. Upon nanotubes sensing element is exposed to $NH_3$, the electrical resistance of the sensors was found to increase. Yoon Taek Jang et al (2004) reported that the resistance of test sample has slowly recovered to its original state with the typical recovery time was 20 hours. Heating treatment in argon atmosphere exposed to sensor at $100^{\circ}C$ leads to faster recovery time [81].

Mixture carbon nanotubes with $SnO_2$ can be used as active sensing component in gas sensing application. In order to get MWCNTs coated $SnO_2$, purified nanotubes was dispersed in $SnCl_2$ solution mixture with HCl. The precipitate was separated from the mother liquor by centrifugation. The coating process then followed by drying and calcinations respectively. The compound material then dispersed in terpineol to form gas sensing element. The sensing method of this sensor is by observation of film resistivity due to gas exposure over the substrate. This sensor is very suitable for polluting gaseous. The working temperature of MWCNTs coated $SnO_2$ is $335^{\circ}C$ [82].

Carbon nanotubes dispersed on polymer composite also can be utilized for sensing application. SWCNTs polymer composite is made of mixing the nanotubes with the ethyl cellulose solution. The mixed solution then was sprayed sensor substrate to form thin films. It was found that polymer mixed nanotubes film exposure to benzene and ethanol affect its resistivity. Higher gas concentration exposed to the film results in higher film resistivity. The response time to identify gas using material is reported of about 100 seconds [8].

### 2.7.3 Ionization

Another technique to identify gas is through gas ionization technique. The gas ionization takes place in between anode and cathode which is connected to high voltage power supply. Since breakdown voltage due to gas ionization occurs at particular value, the voltage fingerprint can be used for gas identification. The utilization of vertically aligned carbon nanotubes as anode results in the lowering of the breakdown voltage due to high linear electric field near nanotubes tips. This hastens breakdown process because of the formation of conducting filament of highly ionized gas surround nanotubes tips. The conducting filament promotes the formation of electron avalanche that bridges the gap between the electrodes and allows a self sustaining interelectrode discharge to be created at low voltages [83]. The gas breakdown voltage will be discussed in more detail in the following section

## 2.8 Theory of Gas Breakdown Voltage

### 2.8.1 Field Emission on Metallic Surface

Electron on metal surface may leaves when it is subjected to heat or radiated with light. Certain threshold electron energy should be possessed or added to the electron in order to be able to escape from metal. The energy then named as the work function and denoted by $\phi$. The work function value is affected by temperature, surface condition and the direction of crystallographic axes. The required minimum energy by the electron to

escape from metal is $E_F + \phi$ where $E_F$ is Fermi energy. This energy should be available as kinetic energy [84].

There are three mechanisms that distinguish electrons released from metal surface, specifically thermionic emission, field assisted thermionic emission, and field Emission. With thermionic emission, the electron will be released from metal surface as the energy in the form of heat is subjected to metal. The current density of thermionic emission is calculated using Richardson-Dushman equation as shown in equation 2.9.

$$J = (1 - R)B_0 T^2 \exp\left(-\frac{\phi}{kT}\right) \qquad (2.10)$$

Where :       J : Current density       $B_0$: 1202 mA/mm$^2$K$^2$

               R: reflection coefficient       T: Temperature

Field assisted thermionic emission occurs in the presence of a strong electric field in the heated metal. The metal work function in this mechanism is reduced due to strong electric field presence and the current density is given by equation 2.10.

$$J = B_0 T^2 \exp\left[-\frac{(\phi - \beta_s E^{\frac{1}{2}})}{kT}\right] \qquad (2.11)$$

Where:       $\beta_s$ : 3.79x10$^{-5}$ (eV/V $^{\frac{1}{2}}$ m $^{-\frac{1}{2}}$) ,

               E: Electric field

In ambient temperature, the electron still can be released from metal surface in the presence of high electric fields. The current density for field emission is calculated by Fowler Nordheim formula as given by equation 2.11.

$$J = \frac{e^3 E^2}{8\pi h \phi} \exp\left\{ -\frac{4}{3}\left(\frac{2m}{\hbar^2}\right)^{\frac{1}{2}} \frac{(\phi - E_F)^{\frac{1}{2}}}{eE} \right\}$$

(2.12)

Where:       m: electron mass ($9.10938188 \times 10^{-31}$ Kg)

h: Planck constant ($6.626068 \times 10^{-34}$ m$^2$ kg/s)

$\hbar$ : $h/2\pi$

The electric field over metal surface is affected by tips radius of surface imperfection. The smaller radius will result in higher electric field at the tips. This effect is called as field intensification factor and denoted as β. The intensification factor is affected by the height and the radius of the tips [85].

### 2.8.2   Gas Ionization

The process of liberating an electron from a gas molecule with the simultaneous production of a positive ion is called ionization. Ionization mechanisms transpire due to either collision, photo ionization or the secondary ionization process between electron and molecules. In the process of ionization by collision, a free electron collides with a neutral gas molecule and gives rise to a new electron and new positive ion. When an electric field applied on two parallel electrodes at low pressure gas column, any electron at the electrode would be accelerated. Collision occurs between electron and gas molecule during the travel toward the anode. If the energy gained during the travel between collisions exceeds the energy required to dislodge an electron from its molecular atomic shell, then ionization takes place. On the ionization attributed by light, the ionization occurs when the amount of radiation energy absorbed by an atom or molecules exceed ionization potential. Secondary ionization occurs after collision ionization or photo ionization takes place. Positive ions are formed due to ionization. If the total energy of positive ion is greater than twice the work function of the metal, then one electron will be ejected and secondary electron will neutralize the ion [86].

### 2.8.3    Gas Breakdown Voltage

Electrical breakdown of the gas occur due to the regeneration of secondary electrons attributed by electron multiplication at low gas pressure under sufficient high electric field. Each primary electron results in a secondary electron. The breakdown voltage does not occur instantly although the applied electrical field has the critical magnitude to regenerate secondary electron. The time interval from the instant of application of voltage to complete breakdown is called time lag. The lag arise out of two reasons specifically, initial electron require time to be in a favorable position in the gap to lead avalanche process and electrons require to build primary avalanche and succeeding generation that leads to a current rise at breakdown [85].

Hassouba found that gas breakdown voltage is influence by cathode material in the electrodes. The measurements show that lower breakdown potentials are associated with lower work function of the cathode material. in addition, he found that he minimum breakdown potential increases with the increase of the work function of the cathode materials [87]. It can be explained that in the material with low work function properties, the electron will able to release from the surface of the material on influence relatively low electric field. The released electron will then collide with the gas molecule in the electrode which further leads to ionization.

Gas compositions on the electrodes highly influence the gas breakdown voltage. Penning effect explain that addition of any gas to a pure gas is able to reduce gas breakdown voltage. One of the examples is the addition of small amount argon to neon which lead to reduction breakdown voltage argon and neon. The reason of reduction of gas breakdown voltage is that the lowest excited state of neon is metastable. The metastable atoms have a long life in neon gas, and on hitting argon atoms there is a very high probability of ionizing them [88].

Gas breakdown voltage is also influenced by the distance of interelectrode separation. In the breakdown field strength is inversely proportional to the distance of interelectrode separation. The closer distance of the interelectrode separation, the higher field strength will produce in the electrode [88]. Hence, due to the higher electric field over the cathode, the electron going to be easier to release from the cathode surface and gain the energy for moving to anode. Furthermore, the electron will gain energy in the influence of high electric field which further able to ionize gas once collision with gas molecule take places

# Chapter 3 : Experimental Procedure

## 3.1 Introduction

This chapter will describe the research methodology of this work followed by explanation of carbon nanotubes film substrate preparation, synthesis and characterization respectively. The testing of carbon nanotubes film as active sensing element will be explained at the end of this chapter.

## 3.2 Methodology

This section describes experimental method of substrate preparation, synthesis, characterization and testing of carbon nanotubes film as an active component on ionization based gas sensing application. The flow chart of the experimental procedure is shown in figure 3.1.

In this work, carbon nanotubes film was grown over oxide layer of cleaned silicon wafer substrate. The dioxide layer was prepared in two different thicknesses in order to study the effect of the layer thickness to carbon nanotubes structure. The utilization of iron and nickel catalyst film with different catalyst treatments over oxidized silicon substrate was aimed to know how the catalysts and its treatment affect the nanotubes structure. The synthesis of carbon nanotubes prepared from two different catalysts with various catalyst treatments are carried out in the same synthesis parameters. The structural properties of synthesized nanotubes were examined using Raman spectroscopy, SEM and TEM. In addition, the electrical properties of carbon nanotubes film were examined by Van der Pauw and Hall Effects technique. The testing of high crystalline nanotubes film as active

component in gas sensor was carried out in testing chamber using ionization mechanism. The complete process of this work will be described in detail in following sections.
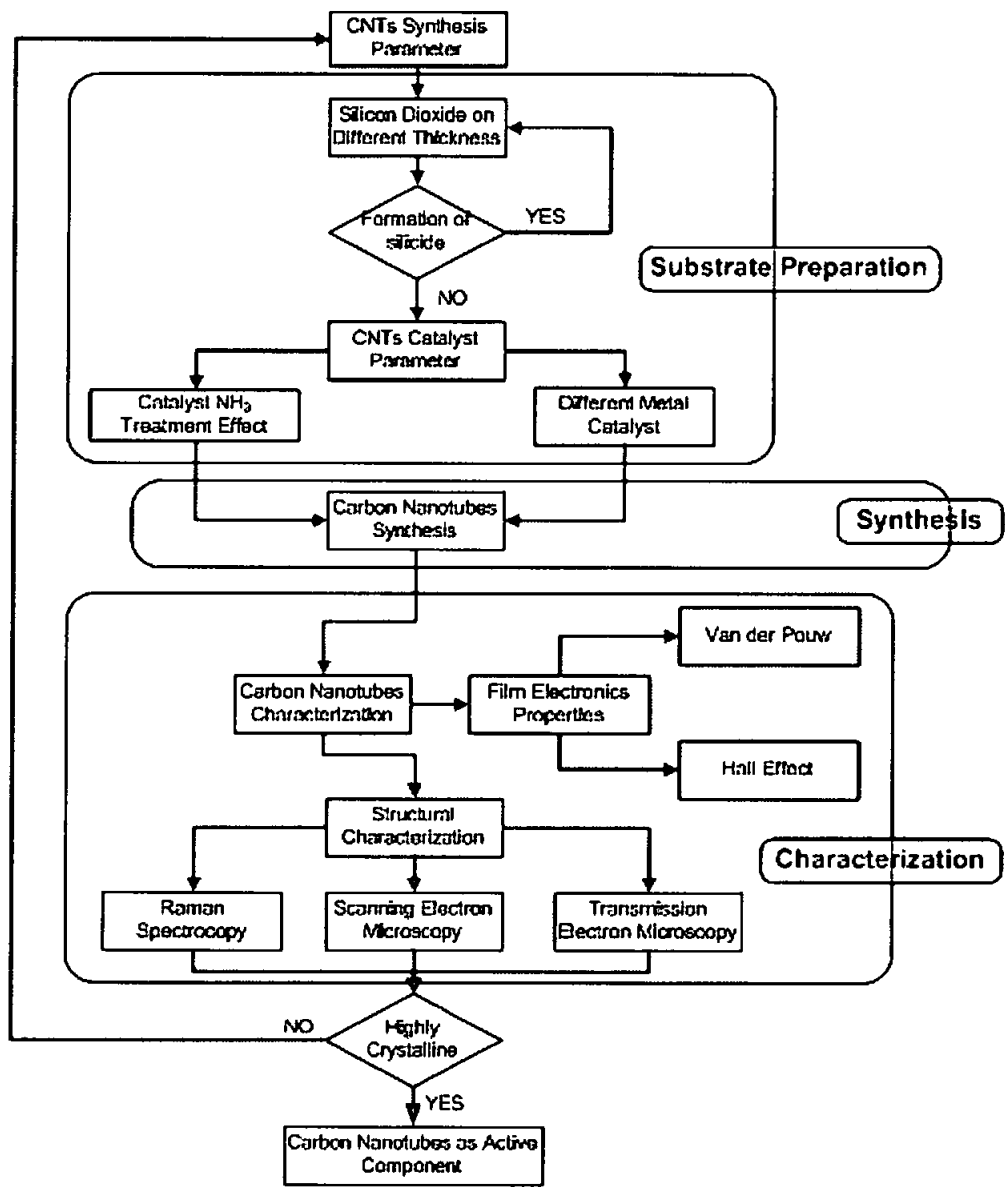


Figure 3-1 Flow chart of synthesizing high crystalline carbon nanotubes film.

## 3.3 Substrate Preparation

The silicon wafer substrate was prepared using standard RC cleaning procedure. The cleaning process is necessary to remove any contaminants over the wafer substrate such as dust, organic contaminant or metallic ion which able to obstruct carbon nanotubes synthesis.

The first stage of RCA cleaning procedures is to remove residual organic contaminants particle over the wafer. This process was started by immersing the wafer into $H_2O/H_2O_2/NH_4OH$ solution for 15 minutes. The solution was prepared by mixing 60 mL $NH_4OH$ (27%) and 300 mL of $H_2O$. The dissolved ammonia hydroxide then heated to $70 \pm 5°C$. Once the mixing solution reached set point temperature, 60 mL of $H_2O_2$ (30%) was added to the solution. In order to remove ammonia peroxide, the wafer was soaked in $H_2O$. Dissolve HF solution was introduced to silicon wafer after removing organic contaminant process to remove native oxide layer on the wafer. Removing ion and metallic contamination particle from wafer was the final stage of RCA cleaning procedures. This stage was carried out by immersing the wafer into $H_2O/H_2O_2/HCl$ solution for 15 minutes. The solution was prepared by mixing 50 mL HCl (37%) with 200 mL $H_2O$ in a Pyrex beaker followed by heating up to $70 \pm 5°C$ over hot plate heater. After removing from the heater, $H_2O_2$ (30%) was added into dissolved hydrochloric acid solution. The wafer was washed by $H_2O$ in order to remove residual hydrochloric acid the substrate.

The silicon dioxide layer was grown over cleaned silicon wafer. The oxide layer is required to prevent metal catalyst film reacts with silicon wafer which lead to silicide formation. Dry oxidation technique was chosen rather than wet oxidation technique in order to obtain better quality of silicon dioxide layer. The relation between dioxide layer thickness and oxidation time is shown in figure 3.2.
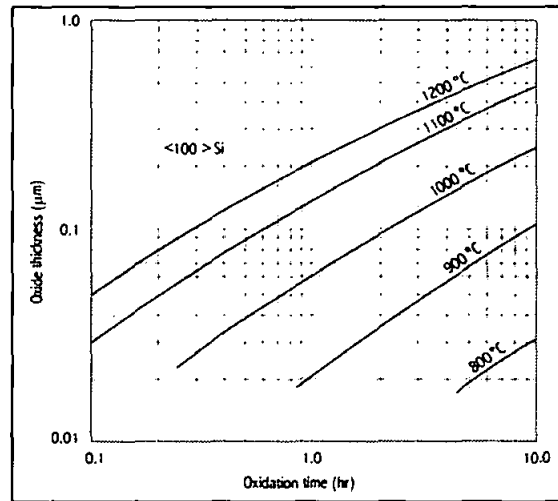
Figure 3-2 Silicon wafer thickness dry oxidation graph [89].

Dry oxidation process is started by heating furnace temperature to 1100°C. While heating to the set point of oxidation temperature, the furnace tube was soaked with argon gas. The aim of this process was to remove contaminant inside the tube and to create inert atmosphere. The inert atmosphere inside the tube was necessary to prevent prior formation of oxide and nitride layer over silicon wafer by ambient oxygen and nitrogen respectively. When the furnace temperature reached 1100°C, the $O_2$ gas is introduced into the furnace tube for the oxidation process to start. The oxidation is performed at two different time, 60 minutes and 210 minutes respectively as shown in figure 3.3 and figure 3.4. Argon gas is introduced into the furnace after the oxidation process to stop the oxide from further growth.
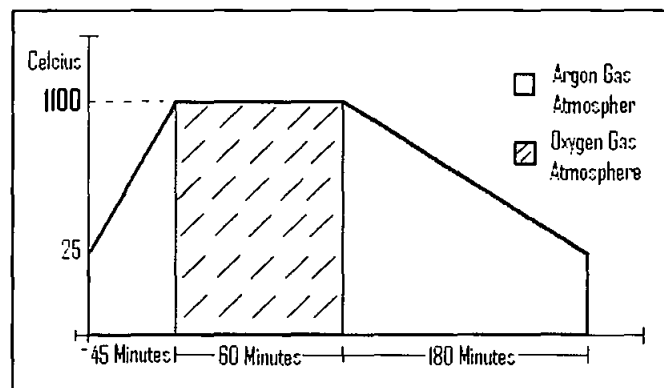


Figure 3-3 Silicon wafer oxidation process schematic for 60 minutes.
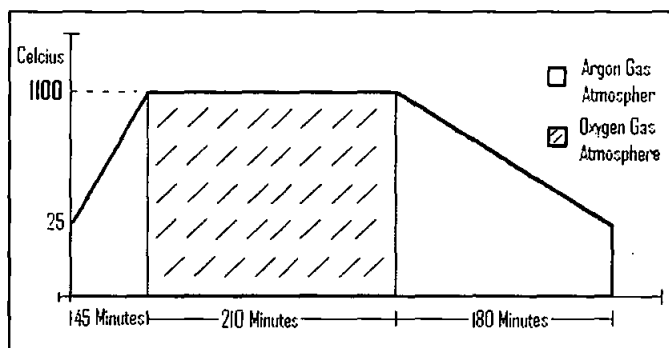
Figure 3-4 Silicon wafer oxidation process schematic for 210 minutes.

## 3.4 Catalyst Preparation

The metal catalysts films were deposited over oxidized silicon wafer using electron beam evaporator in the pressure of about $3 \times 10^{-5} - 5 \times 10^{-5}$ Torr. The coated catalysts substrates were then subjected into two different catalyst treatments. The first group of the catalyst coated substrate was loaded into thermal CVD furnace directly for synthesizing process without any $NH_3$ etching treatment whilst the second group was annealed in $NH_3$ atmosphere at 800°C for 20 minutes prior to nanotubes synthesis. Heating up the substrate to 800°C and cooling down to ambient temperature was carried in argon atmosphere. Flushing furnace chamber by argon gas prior to substrate annealing was to ensure there were no trapped contaminants particle inside the chamber and there were no reaction between catalysts and undesired gases during heating, annealing and cooling down process. The time frame of ammonia annealing process is shown in figure 3.5.
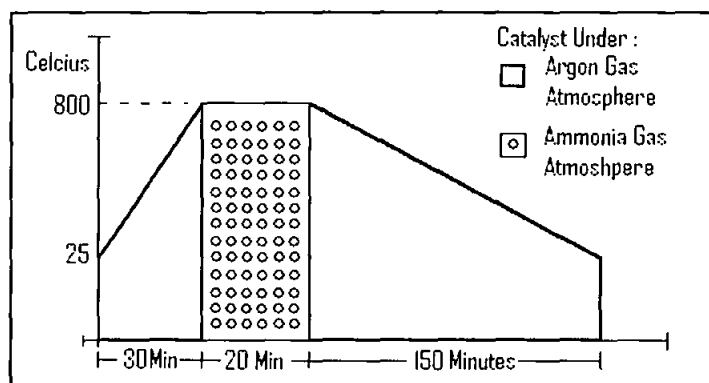


Figure 3-5 Catalyst annealing process over argon and ammonia atmosphere.

## 3.5 Carbon Nanotubes Synthesis

The synthesizing carbon nanotubes film was carried out in quartz tube of 8 cm in diameter and 40 cm in length. Prior to loading catalyst coated substrate into thermal CVD furnace, the furnace tube was soaked by argon flow rate of 500 sccm for 5 minutes to remove contaminant such as dust from quartz tube. The substrate was placed in furnace tube followed by heating to 700°C in argon gas atmosphere. Argon gas was required to remove trapped oxygen and nitrogen inside the tube and create inert atmosphere. Hydrogen with the flow rate of 500 sccm was soaked over catalytic coated sample for 10 minutes prior to MWCNTs synthesis. The substrate reduction process by hydrogen convert $Fe_2O_3$ and $Fe_3O_4$ become Fe particle over $SiO_2$ substrate. The nanotubes synthesis was carried out by decomposition of ethylene for 10 minutes at 700°C. Cooling down as synthesized nanotubes to 300°C and room temperature was carried out sequentially in hydrogen and argon atmosphere respectively. The time sequence diagram of synthesizing nanotubes is shown in figure 3.6 whilst the CVD furnace quartz tube is shown in figure 3.7.
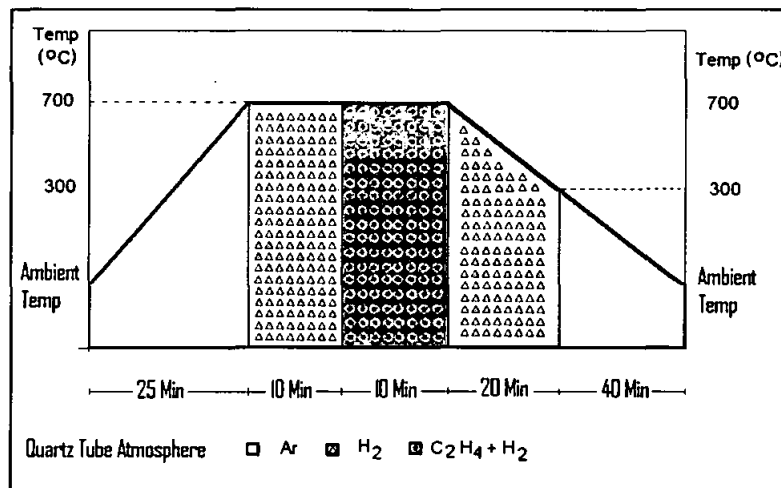


Figure 3-6. Carbon nanotubes synthesis process sequence.
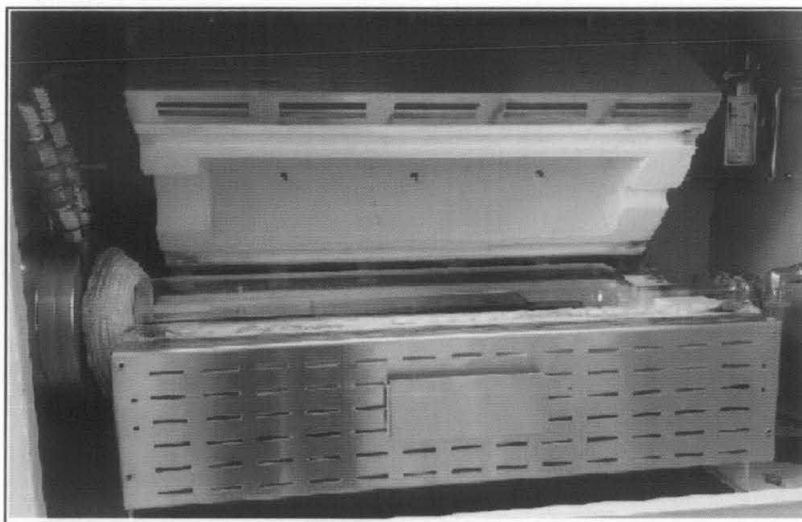
Figure 3-7 Thermal CVD furnace tube.

## 3.6 Scanning Electron Microscopy

Carbon nanotubes film is assembled of billion individual tubes in nano size diameter, therefore the film surface morphology and its cross sectional image is not able to be examined through visible light optical microscope. Consequently, higher magnification microscope is required to capture image from the nanotubes film. Since SEM use shorter wavelength than the optical microscope to capture image from the sample, higher image magnification can be obtained by SEM.

### 3.6.1 Image Capturing Technique

The preparation of SEM sample commonly is started by coating the sample with conductive material. Since carbon nanotubes film already conductive, sample coating with conductive material is not required prior to image capturing. The nanotubes film placed inside SEM vacuum column and adhered to sample holder using conductive carbon tape. High vacuum was highly necessary to prevent interaction between electrons and air particle which impede image capturing from the sample since the image captured due to interaction between electron and the sample. Air inside the SEM chamber was evacuated using vacuum pump until the chamber pressure reached of $10^{-6}$ mbar. In order to capture finest image from the sample, low speed image scanning mode was maintained

while capturing image. Leo 1525 model was used to capture image from carbon nanotubes film. The SEM picture is shown in figure 3.8
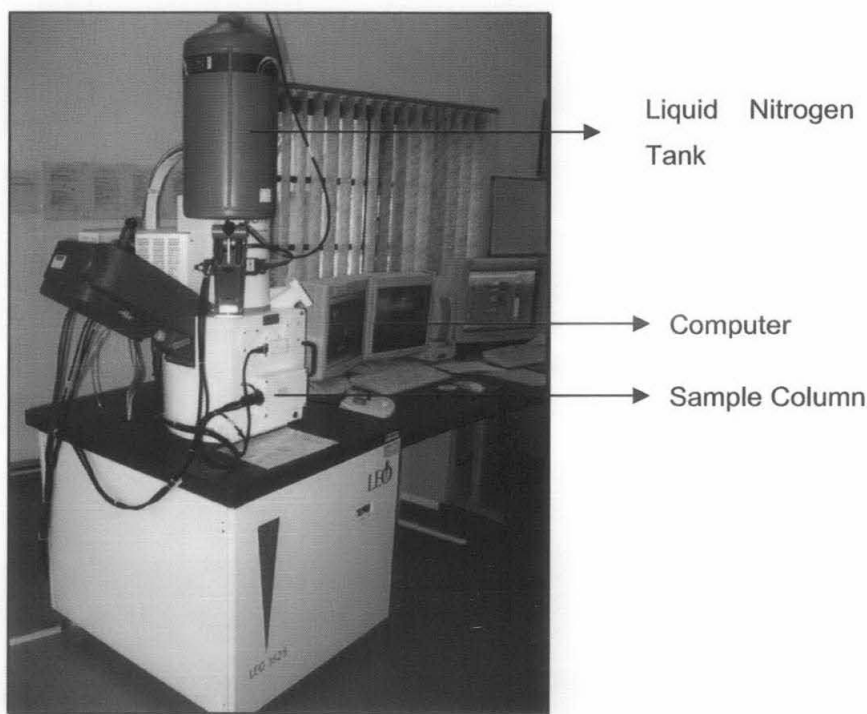


Figure 3-8. Leo 1525 scanning electron microscopy.

## 3.7 High Resolution Transmission Electron Microscopy

The carbon nanotubes sample was then observed using TEM to measure its outer and inner diameter. Since TEM resolution is capable up to 0.144 nm, the defect inside nanotubes layer can be disclosed through TEM image analysis. The analysis of TEM image can also be use to reveal growth type of carbon nanotubes, specifically base or tip growth type. In this work TEM image was captured using Tecnai 20 transmission electron microscopy.

### 3.7.1 Sample Preparation for TEM Observation

Since carbon nanotubes grown over silicon substrate were on agglomerate form whilst TEM characterization has to be carried out on thin film, the nanotubes should be

dispersed over copper grid to form thin film prior to TEM observation. The nanotubes were dissolved into isopropanol solution followed by sonification for 15 minutes in ultra sonic bath. A drip of the solution placed over receptacle copper matrix in ambient temperature and atmospheric pressure for drying process. The nanotubes image capturing was carried out inside TEM chamber at $10^{-6}$ mbar in pressure. TEM image of crystalline material was obtained mainly through diffraction mechanism between electron and atom. Since the diffraction intensity depends on the orientation of crystal atoms planes relative to the electron beam, specimen holders was tilted to variety of angles to obtain specific diffraction conditions which results in the clearest nanotubes image.

## 3.8 Structural Characterization using Raman Spectroscopy

Raman spectroscopy is a preeminent tool to investigate carbon nanotubes properties since SWCNTs diameter, chirality, electronics properties, crystallinity, and sample homogeneity revealed through carbon nanotubes Raman spectra analysis. Furthermore, Raman spectra of carbon nanotubes can be obtained rapidly in ambient room temperature and atmospheric pressure without any sample preparation which may cause damage to the sample.

### 3.8.1 Carbon Nanotubes Spectra Measurement

Raman spectroscope uses visible light emitted from laser to investigate spectra of any samples. The laser is utilized to excite electron from ground state to virtual state through scattering process between photon and electron of a sample. The scattered photon passes notch filter before detected by CCD detector. The signal processing system then process the signal obtained from detector. In most Raman spectroscope, microscope is attached to the spectroscope in order to reduce fluorescence during Raman spectra measurement on the sample [90].

The calibration of Raman spectroscope prior to acquire Raman spectra is to obtain precise spectra. The first stage of calibration was adjustment of spectra shift. The aim of

this stage was to ensure spectra peak only occur in appropriate frequency shift. The calibration of Raman spectra detector was carried out after spectra shift calibration. The detector calibration was aimed to guarantee that detector only acquire laser with specific wavelength. The final stage of Raman spectroscopy calibration was test out the signal intensity which can be acquired by detector. Standard bare silicon wafer was utilized as testing material in calibration process. If the frequency peak acquired from silicon wafer was the same with standard Raman frequency shifting for silicon, the Raman spectroscope ready to be used for carbon nanotubes characterization tool.

Structural characterization of carbon nanotubes was carried out by Raman spectroscope (Horiba Jvon). The frequency shifting was traced in the range of 100 cm$^{-1}$ to 1800 cm$^{-1}$ with laser excitation energy of 2.41 eV. The sample was exposed to laser line through 100x focus lens. There was no sample preparation applied to pristine carbon film prior to acquire the Raman spectra. Raman spectroscopy is shown in figure 3.9
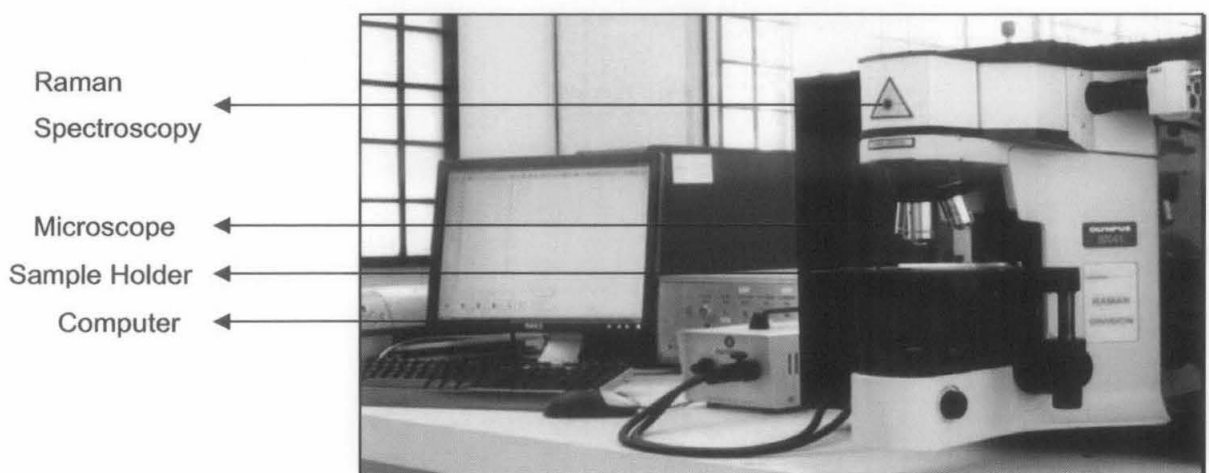


Figure 3-9 Raman spectroscopy (Horiba Jvon)

## 3.9 Van Der Pouw Film Resistivity Measurement

In order to obtain sheet resistivity of carbon nanotubes film van der pouw measurement technique was applied to the film. Fully automatic I-V meter dedicated for measuring sheet resistance was used to reduce error during measurement hence precise measurement can be achieved.

## 3.9.1 Sample Preparation and Measurement Technique

Van der Pauw technique was carried out by measuring horizontal and vertical resistivity of the sample. In order to reduce ohmic contact as low as possible between sample holder connector and carbon nanotubes film, silver paste was used as medium to connect the film and the connector. Furthermore, the influence of connector resistivity was minimized through short wire connection between sample and measurement system. The wire connection was placed so that they were symmetrical about a line through any pair. Sheet resistivity of carbon nanotubes film was calculated through I-V curve measurement of $V_{34}$ vs $I_{12}$ and $V_{14}$ vs $I_{23}$ to obtain $R_A$ and $R_B$ value, respectively. The sheet resistivity can be calculated and obtained using equation 3.1.

$$R_s = \left( \frac{\pi d}{\ln 2} \right) \left( \frac{R_a + R_b}{2} \right)$$

(3.1)

where :    $R_a = V_{34} / I_{12}$

$R_b = V_{14} / I_{23}$

The schematic of wire connection to I-V meter and sample holder is shown in figure 3.10 and figure 3.11 respectively.
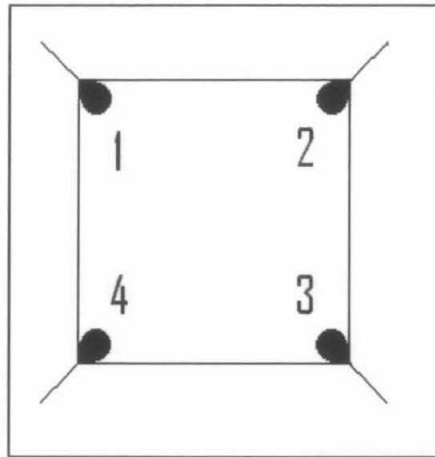
Figure 3-10 Van der Pauw measurement connection
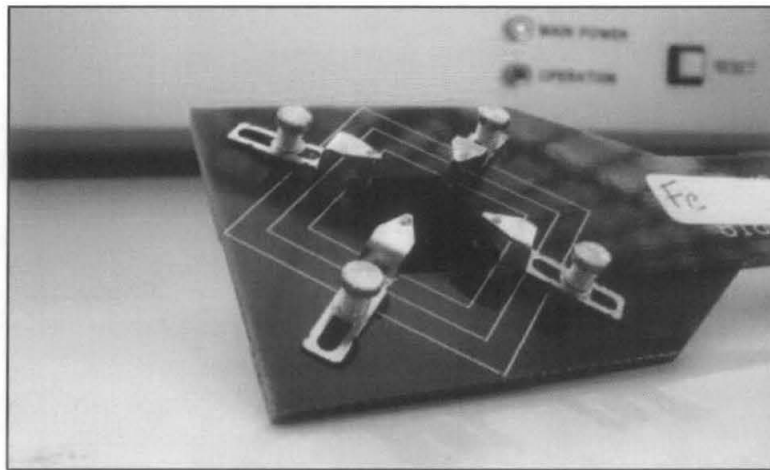


Figure 3-11 Sample connection on Van der Pauw resistivity measurement.

## 3.10 Hall Effect Electron Mobility Measurement

Hall Effects measurement on carbon nanotubes film was carried out to reveal charge mobility on the sample. The mobility was quantified using Ecopia Hall Effect measurement system as shown in figure 3.12.

Measurement
System
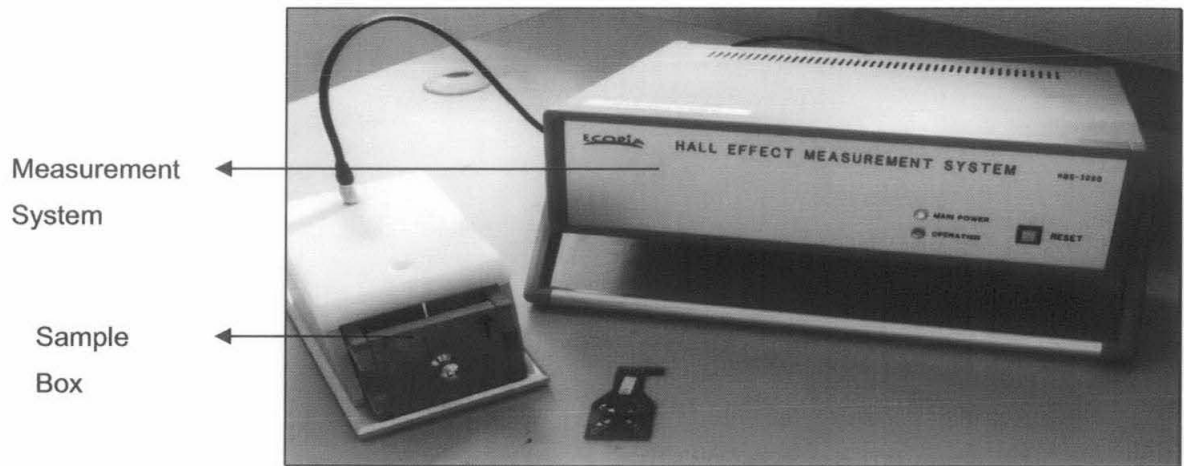
Sample
Box

Figure 3-12 Ecopia Hall Effect measurement device

### 3.10.1 Sample Preparation and Measurement Technique

The measurement was started by quantify sheet resistance of carbon nanotubes in the absence of perpendicular magnetic field pass the film. The ohmic contact between nanotubes film and sample holder connector was minimized through silver paste soldering. The electron mobility of carbon nanotubes film was measured by placing 0.510 Tesla magnetic fields perpendicular to the nanotubes film with diagonally current injection on the film. This current was required to generate hall voltage across the film. Schematically, Hall Effect measurement configuration is shown in figure 3.13.
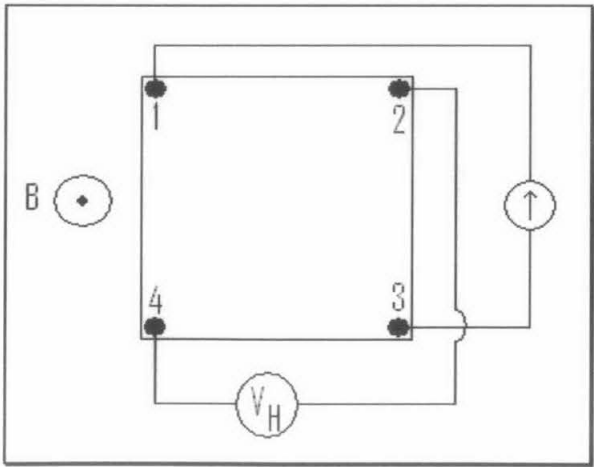


Figure 3-13 Hall Effect measurement configuration.

Hall voltage was obtained by applying current to the edge number one and three ($I_{13}$) whilst the measurement of voltage was carried out in edge number two and four ($V_{24p}$) in the presence of positive magnetic field. The opposite Hall voltage ($V_{42p}$) was obtained by applying reverse current to edge number three and one ($I_{31p}$). The measurement of $V_{13P}$ and $V_{31P}$ with $I_{42}$ and $I_{24}$, respectively, ware carried out with the same technique. In order to obtain $V_{24N}$, $V_{42N}$, $V_{13N}$, and $V_{31N}$. reserve magnetic field was applied to the sample. The Hall Effect measurement was carried out in room temperature with the absence of light.

## 3.11    Gas Ionization Sensor using Carbon Nanotubes Film Testing

Electric field in between anode and cathode can be generated by connecting conductive electrodes plate to voltage source. The electric field over electrodes surface is affected by its geometry. The rougher surface and the smaller tips lead to higher electric field. Since carbon nanotubes have high aspect ratio and have tiny dimension, the carbon nanotubes film is able to create high electric field over the cathode.

On very high electric field, electron on the cathode is able to release from its orbital. The released electrons gain energy from the electric field to move along the electrodes. In non elastic collisions between electrons and gas molecules on the electrodes, the internal energy level of gas molecule changes. In state of electron energy exceeds ionization potential of a gas molecule, gas ionization occur in the electrodes. The ionization potential is unique in wide range of gases. This property can be used for sensing presence of any gas.

The schematic of gas sensing application based on ionization method using carbon nanotubes film is shown in figure 3.14.
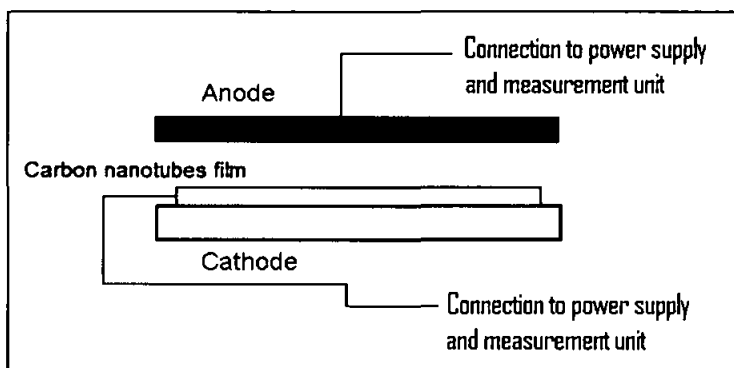
Figure 3-14 Carbon nanotubes as active component on gas sensor.

The active component of gas sensor was made of carbon nanotubes film cathode and aluminum (99%) film anode. Carbon nanotubes film used in this experiment was 10 mm x 10 mm in size whilst the typical individual nanotubes diameter length of about 18 to 40 nm with length of about 1.5 μm.

### 3.11.1 Gas Sensor Apparatus Setup

In order to test carbon nanotubes as active component on gas sensing application, prepared MWCNTs film was placed inside gas testing vacuum chamber made of stainless steel. The chamber was connected to oil free turbo vacuum pump for evacuating air inside the camber prior to testing. Moreover, vacuuming process aim to ensure there was no other contaminant gas involve during the testing. The active component of gas sensor was connected to ammeter and variable DC high voltage power supply capable of 500 V. In order to reduce as low as possible ohmic contact between MWCNTs film and wire, silver paste was used as connector instead standard tin. The gap between MWCNTs anode film to metallic film was controlled by high precision micrometer connected to the electrodes holder. The volume of flown gas into chamber was measured and controlled through gas flow controller. In order to identify gas breakdown voltage, ammeter was serially connected to high voltage power supply whilst volt meter was connected parallel. Schematically, the testing process is shown in figure 3.15 whilst complete setup is shown in figure 3.16.
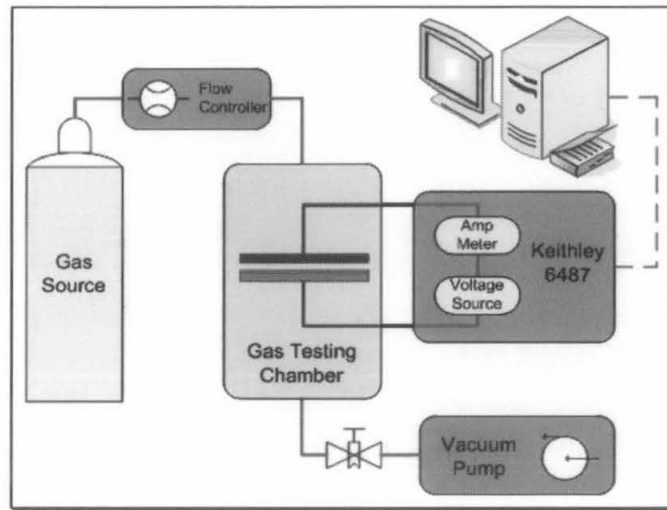
Figure 3-15 Gas sensor testing schematic.
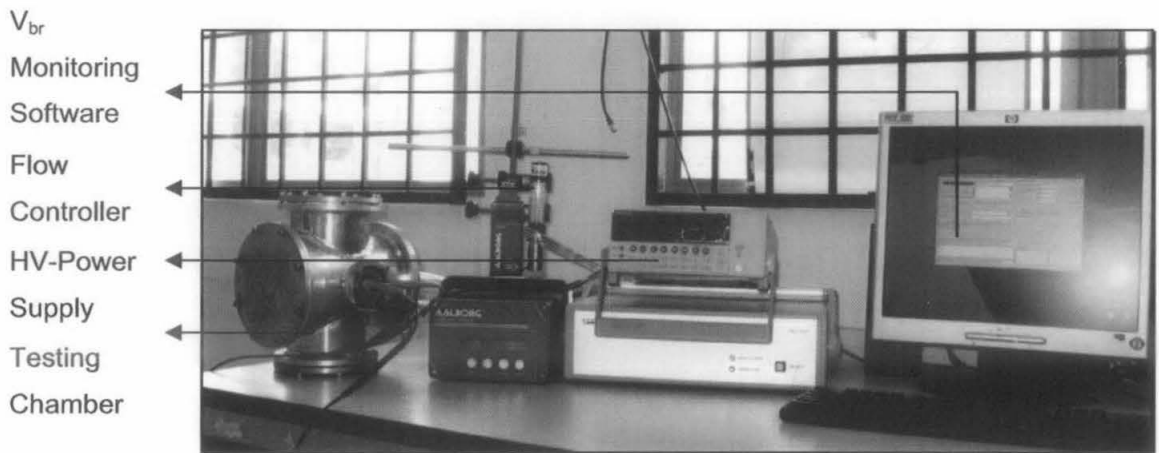


Figure 3-16 Complete setup of carbon nanotubes based gas sensor testing.

## 3.11.2 Gas Sensor Testing Process

Prior to testing process, gas testing chamber was vacuumed. The process then continued by flowing gas into testing chamber which is controlled by gas flow controller. High voltage power supply connected to the electrodes was increased gradually until breakdown voltage occurs. The voltage was switched off promptly once gas breakdown voltage detected in between the electrodes.

# Chapter 4 : Results and Discussions

## 4.1 Introduction

This chapter will explain the result and discussion of this work. The discussion is started by the explanation of silicon oxide thickness effect to carbon nanotubes morphology followed by the discussion of catalyst effect to nanotubes structure using SEM. The discussion then continued by revealing the effect of carbon nanotubes catalyst and its treatment to nanotubes structure using Raman spectroscopy. In addition, the effect of catalyst to nanotubes structure will also be disclosed using TEM analysis. The resistivity and electron mobility of carbon nanotubes film will be discussed through Van der Pauw and Hall Effect technique analysis. The results of testing carbon nanotubes film as active sensing element on ionization based gas sensing will be discussed of this chapter.

## 4.2 Scanning Electron Microscopy Analysis of CNTs Film

The morphology of carbon nanotubes grown over various substrate preparations are presented in this section. The discussion was begun with the observation of carbon nanotubes yield as the effect of oxide thickness. The effect of utilization iron and nickel catalyst film to nanotubes film morphology was also discussed. The morphology of the nanotubes film was revealed through SEM images.

## 4.2.1 Effect SiO₂ Layer Thickness to CNTs Film Morphology

The analysis of carbon nanotubes grown over two different thickness of silicon dioxide layer is presented. The oxide layer of the first substrate was prepared by 60 minutes

oxidation whilst the second substrate was prepared by 210 minutes oxidation. The estimated thickness of oxide layer grown over silicon substrate according to silicon oxidation chart was about of 100 nm and 200 nm respectively. Carbon nanotubes grown on two different substrates are shown in figure 4.1 and figure 4.2.

Figure 4-1 shows carbon nanotubes and granular particles formed over the substrate. EDX measurement reveals that the granular particles are mainly composed of silicon and iron compounds. The formation of iron silicide particle is due to insufficient silicon dioxide layer to prevent reaction between deposited iron film and silicon wafer while synthesizing carbon nanotubes. Although silicon dioxide layer have been formed over silicon substrate, heavy reduction process in high temperature ammonia and hydrogen atmosphere prior to carbon nanotubes synthesis are expected to etch the oxide layer and further exposed the underlying silicon layer. The absence of silicon dioxide layer as buffer layer causes metal catalyst to react with silicon substrate. Hence reaction between silicon and iron catalyst at high temperature produces iron silicide and iron compound, which is catalytically inactive that can hinder carbon nanotubes growth [91]. However a number of carbon nanotubes can be observed interposed between silicide granules. The small amounts of carbon nanotubes grown in between silicide are due to iron clusters attached to iron silicide [92].
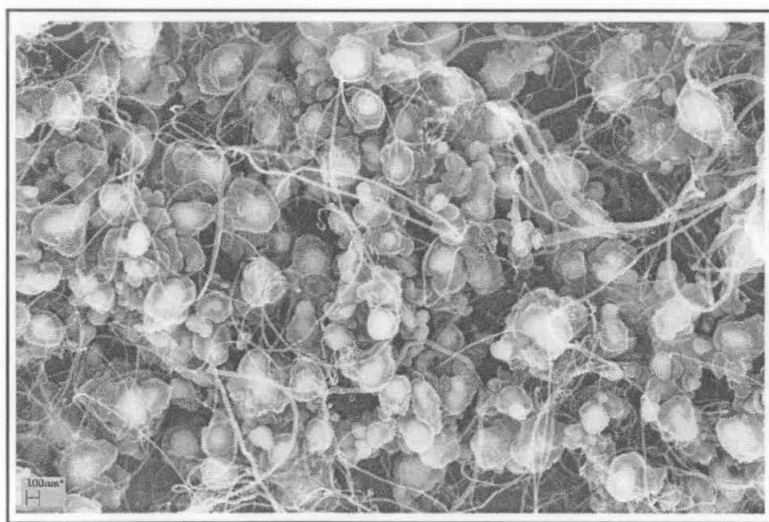


Figure 4-1 Carbon nanotubes grown over 100 nm SiO$_2$.
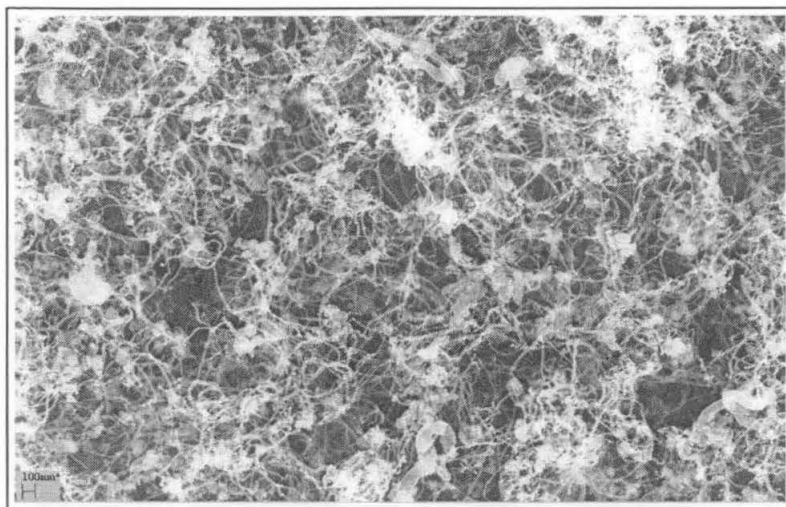
Figure 4-2 Carbon nanotubes grown over 200 nm $SiO_2$.

As notice in figure 4.2, thicker silicon dioxide layer (200 nm) leads to higher yield carbon nanotubes without any silicide formation. The absence of silicide formation is due to thicker silicon dioxide layer that is sufficient to prevent chemical reaction between iron and silicon wafer. Since iron catalyst film does not react with silicon dioxide at high temperature hydrogen and ammonia atmosphere, the continuous iron thin film transformed into isolated catalyst islands [93]. Due to chemical stability, iron particles become saturated or supersaturated with carbon atoms at the growth temperature. This condition allows precipitation of carbon from the surface of the iron particle which leads to the formation of tubular carbon solids in $sp_2$ structure [91].

### 4.2.2 Catalyst Effect on Carbon Nanotubes Growth

Structure and morphology of carbon nanotubes are highly influenced by the metal catalyst used and synthesis technique. The effects of various metal catalysts to nanotubes morphology grown using thermal CVD technique were examined through utilization of iron and nickel as the catalysts. Field emission scanning electron microscopy (FESEM) images of carbon nanotubes grown over iron and nickel catalyst are shown in figure 4.3 and figure 4.5 whilst higher magnification image of iron and nickel catalyzed carbon nanotubes grown are shown in figure 4.4 and figure 4.6 respectively.
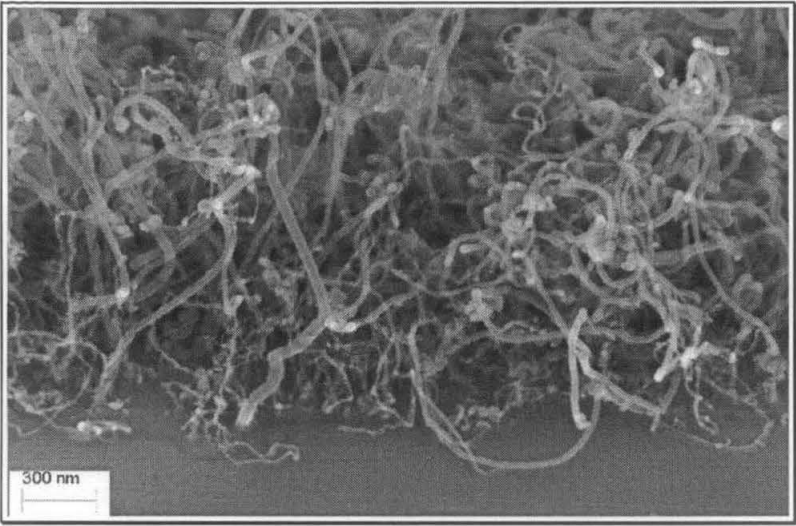
Figure 4-3 Cross sectional view of CNT obtained using iron catalyst.
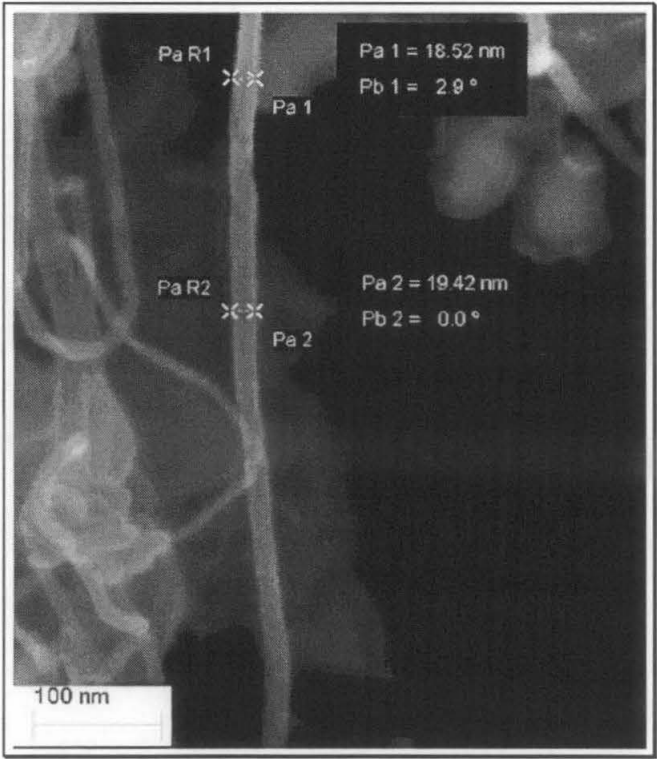


Figure 4-4 Higher magnification of carbon nanotubes grown over iron catalyst film.
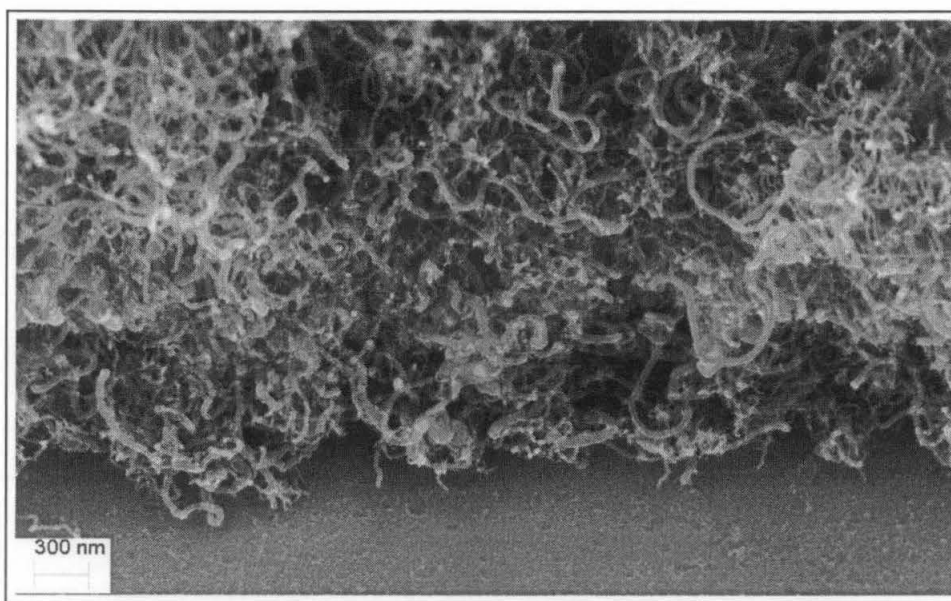
Figure 4-5 Cross sectional view of CNT grown on nickel coated silicon wafer.
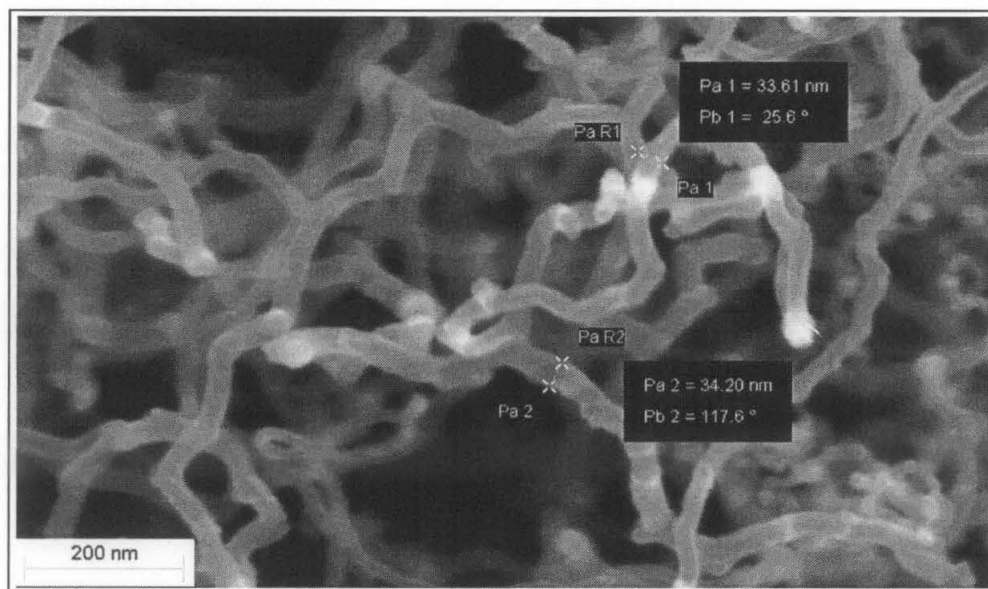


Figure 4-6 High magnification of carbon nanotubes grown over nickel catalyst.

Figure 4-3 and figure 4.4 show cross sectional image of carbon nanotubes grown over iron catalyst at low and high magnification respectively. Figure 4-3 shows carbon nanotubes are some vertically random grown whilst other area of image shows more random growth. From figure 4.3, typical nanotubes lengths grown over iron catalyst film are of about 1.5 µm. The random growth of carbon nanotubes is expected due to the

widely spread nano particle islands resulting in either vertically or horizontally growth of carbon nanotubes. In this experiment wide catalyst island spacing is attributed to ammonia etching treatment. J.I Sohn (2002) found that continuous iron catalyst film transforms into either nano or submicron sized particle islands under ammonia treatment atmosphere of about 800°C. [94]. Figure 4-4 shows smooth shape carbon nanotubes obtained from carbon feedstock decomposition over iron catalyst layer. Visual observation of FESEM indicates that typical diameter of carbon nanotubes is 18 nm. This finding of reasonably narrow diameter carbon nanotubes is agreed with the analysis obtained from Raman spectroscopy.

Figure 4-5 shows carbon nanotubes grown over nickel catalyst coated $SiO_2$ substrate. Carbon nanotubes synthesized over nickel catalyst are found to be more defective than the nanotubes synthesized over iron catalyst film. Nanotubes appear to be curlier compared to the one obtained using iron catalyst.

Higher magnification image of carbon nanotubes grown over nickel film catalyst is shown in figure 4.6. Typical diameters of synthesized carbon nanotubes are measured here is around 34 nm. Nickel catalyst film had deformed into nano catalyst islands after been subjected to ammonia etching process at high temperature. The deformations of catalyst size also take place prior to carbon nanotubes synthesis. Chunnian He et al (2006) show annealing temperature of nickel catalyst particle in hydrogen atmosphere highly influences the nickel catalyst particle size. The annealing of nickel colloid at temperature in the range of 400°C to 600°C in hydrogen atmosphere was reported to increasing nickel catalyst particle to the range of 11 to 15 nm [95].

## 4.3 Raman Spectroscopy

The crystallinity of nanotubes structure grown over iron and nickel thin film with different catalyst treatment is discussed in following section. The discussion is started by elucidating the effect of two metallic catalysts to the nanotubes structure. The discussion of the influence of ammonia etching to nanotubes crystallinity is also discussed.

## 4.3.1 Effect of Different Catalyst on Carbon Nanotubes Structure

The evaluation of nanotubes crystallinity grown on different catalyst layer was carried out by Raman spectroscopy in frequency resonant range of 100 cm$^{-1}$ to 1800 cm$^{-1}$ with laser excitation energy of 2.41 eV. Raman spectrum of carbon nanotubes obtained from iron and nickel catalysts are shown in figure 4.7 and figure 4.8 respectively.
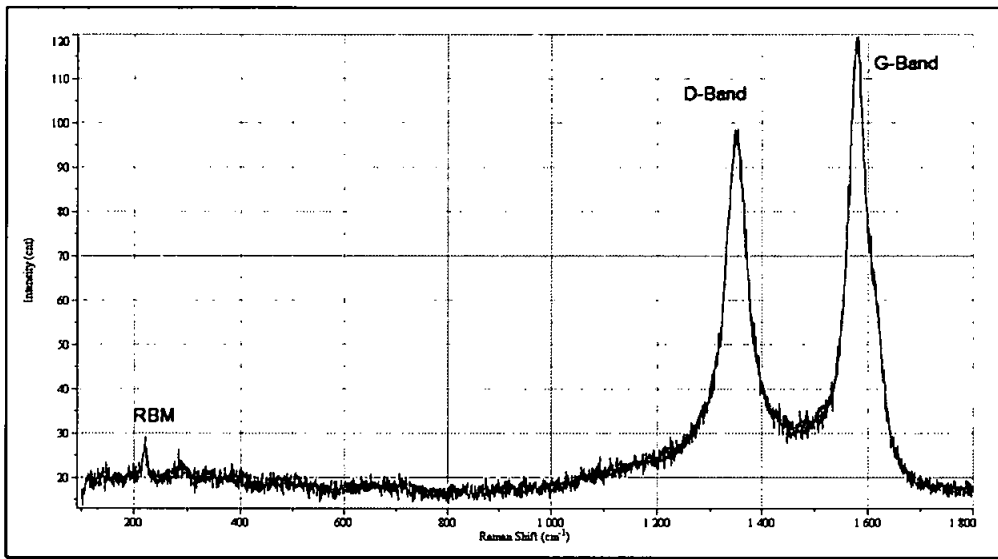


Figure 4-7 Raman spectroscopy of MWCNTs grown on iron coated SiO$_2$ substrate.
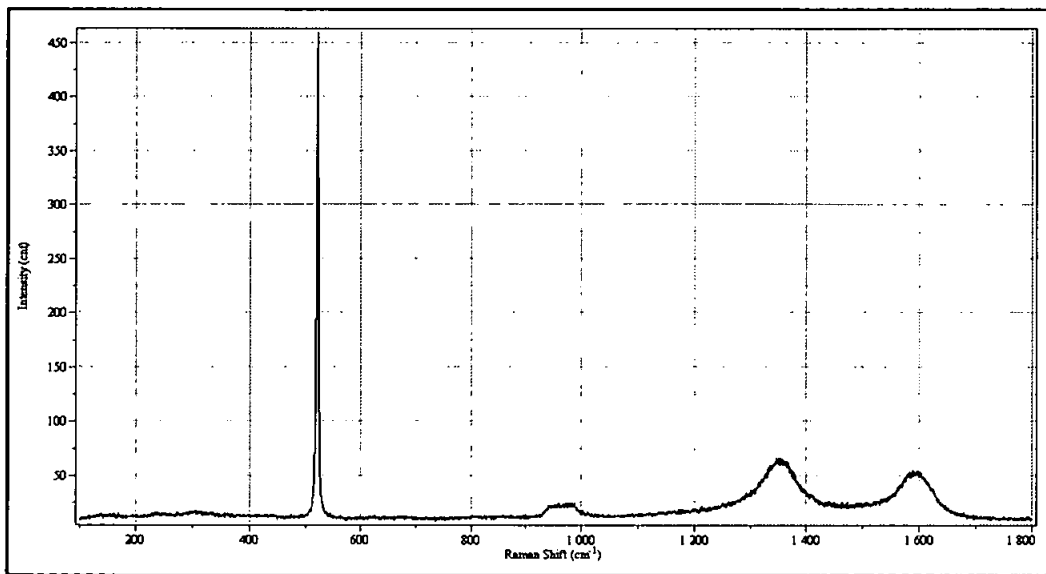


Figure 4-8 Raman spectroscopy of MWCNTs grown on nickel coated SiO$_2$ substrate.

Table 4-1  Raman Detail of MWCNTS Sample Grown on Different Catalysts

| Catalyst | RBM | D-band | G-band | $I_d/I_g$ | $I_g/I_s$ |
|---|---|---|---|---|---|
| Fe | 220 cm$^{-1}$ | 1350 cm$^{-1}$ | 1578 cm$^{-1}$ | 0.83 | 6.83 |
| Nickel | - | 1351 cm$^{-1}$ | 1592 cm$^{-1}$ | 1.13 | 0.12 |

The spectra in figure 4.7 and figure 4.8 show the absence of peak splitting of G-band. The appearance of the G-band splitting in the spectrum is an indication of single walled type of carbon nanotubes. The G-band of SWCNTs consist of two main components, one peak at 1590 cm$^{-1}$ (G$^+$) and the other peak close to 1570 cm$^{-1}$ (G$^-$) [96]. Since G-band peak splitting was not found in the nanotubes spectra, ethylene decomposition over iron and nickel catalyst yield MWCNTs instead of SWCNTs.

Since the D-band on nanotubes Raman spectra arise from its structural defect [64] whilst G-band indicating formation of well graphitized carbon nanotubes [97], the ratio of G-band to D-band ($I_d/I_g$) is commonly used to determine crystallinity of nanotubes sample [20, 51, 98, 99]. From Table 4-1, crystallinity of MWCNTs grown over iron and nickel catalyst layer is $I_d/I_g$ ratio 0.83 and 1.13 respectively. Since utilization of iron catalyst gives lower ratio of $I_d/I_g$ than nickel catalyst, carbon nanotubes sample with iron catalyst gives higher crystallinity nanotubes compared to the one with nickel catalyst. This result agrees with the observation of FESEM image which shows that utilization of iron catalyst gives suave shape nanotubes compared to the nickel catalyst which results in defective nanotubes.

In addition, Young Soo Park et al (2001) suggested that the low intensity ratio of  D-band to G-Band on Raman spectroscopy indicates that nanotubes sample contain a small amount of amorphous carbon [97]. This implies that the synthesis utilizing iron catalyst film yield better quality nanotubes with lower amorphous carbon compared to MWCNTs synthesized over nickel catalyst layer.

The Raman signal appeared as two prominent peaks occurring around 521 cm$^{-1}$ and 1000 cm$^{-1}$. Those peaks originate from the first and second order Raman spectrum of silicon. The first order peak of silicon can be utilized for calibration of nanotubes spectra [62]. Since the silicon peak obtained in spectrum is the same as standard silicon peak, the measurement of nanotubes spectra was carried out accurately. Furthermore the intensity ratio of G-band to first order peak intensity of silicon ($I_g/I_s$) can be utilized to approximate the yield of carbon nanotubes [39]. Obviously, on the spectrum of nanotubes grown over iron catalyst layer, prominent silicon peak is hardly observed. This is to be expected that the silicon substrate is fully covered by densely populated nanotubes. Therefore Raman spectroscopy laser has not been able to penetrate passes the nanotubes layer to produce silicon peak. The intensity ratio of $I_g/I_s$ on carbon nanotubes grown over iron catalyst is 6.83, whilst lower ratio ($I_g/I_s$ = 0.12) is obtained by carbon nanotubes grown over nickel catalyst. Hence utilizing iron as the catalyst will give higher yield of carbon nanotubes compared to the one using nickel catalyst.

Raman spectrum obtained from the nanotubes grown over iron catalyst film shows RBM peak of around 200 cm$^{-1}$. The low frequency of Raman spectra observed in MWCNTs is also suggested from the same origin as SWNT [100]. The presence RBM peak in MWCNTs indicate small diameter of carbon nanotubes. The smaller diameter leads to less number of walls inside the nanotubes. As the consequence, most inner diameter of MWCNTs is able to vibrate which result RBM peak on Raman spectra [100]. The appearance of RBM on MWCNTs sample was also obtained by Y. Ando et al (2002) from MWCNTs produced through Helium DC arc discharge technique [101]. J.M Benoit et al (2002) suggested that the purification method plays an important role since the RBM peak on Raman spectra is only observe on pure nanotubes sample. On unclean nanotubes sample RBM peak could not be observed due to the presence of carbonaceous compound [100]. The presence of RBM peak on the MWCNTs sample implies that the synthesis technique in this work is able to produces nanotubes with less carbonaceous compound.

**4.3.2 Effect of Ammonia Etching on Carbon Nanotubes Structure**

The effect of catalyst etching at high temperature ammonia on the crystallinity of carbon nanotubes through Raman analysis will be discussed in this section. Raman spectrum of nanotubes grown over etched iron and nickel catalyst are shown in figure 4.9 and figure 4.10 respectively.
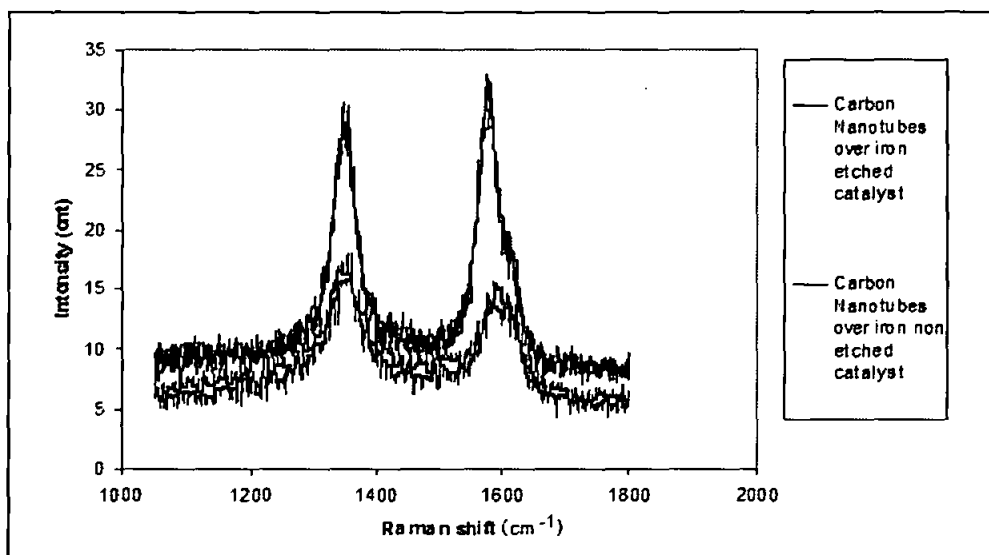


Figure 4-9 Raman spectra of carbon nanotubes grown on etch and non etch iron catalyst.
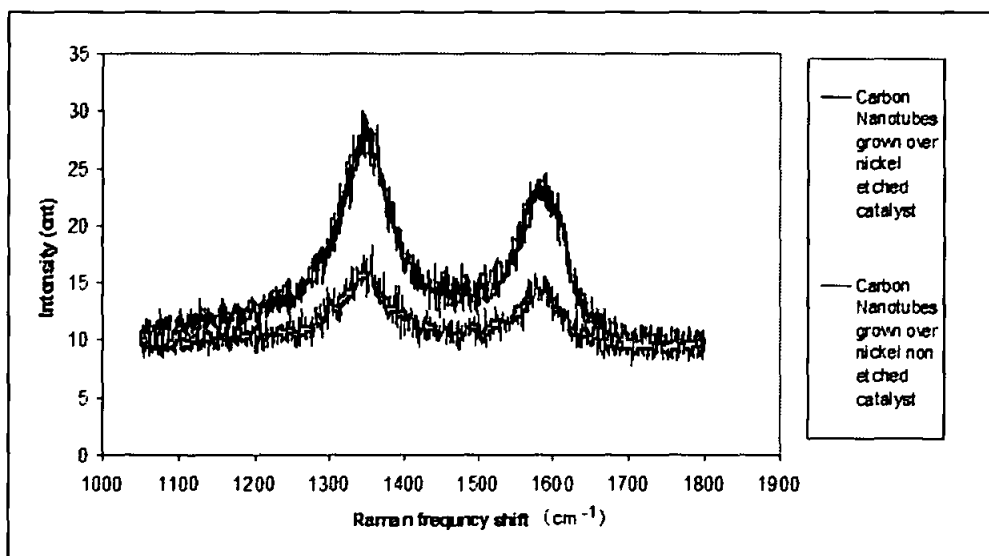


Figure 4-10 Raman spectra of carbon nanotubes grown on etch and non etch nickel catalyst.

Table 4-2 Ratio of $I_d/I_g$ for Carbon Nanotubes Subjected to Ammonia Etching

| Catalyst Treatment | $I_d/I_g$ Ratio | |
| --- | --- | --- |
| | Iron Catalyst | Nickel Catalyst |
| Etching | 0.85 | 1.2 |
| Non Etching | 1.15 | 1.1 |

Table 4-2 shows that carbon nanotubes grown over etched iron catalyst gives the highest crystallinity value whilst non etched iron and nickel catalyst give about the same value. Cheol et al (2002) reported that carbon nanotubes sample with iron catalyst subjected to ammonia etching results in higher crystallinity carbon nanotubes compared to the one obtained from nickel catalyst with the same treatment. Cheol (2002) suggested that low $I_d/I_g$ ratio represents low defective nanotubes as confirmed by TEM which showed high crystalline nanotubes wall [102]. Jung Inn Sohn et al (2002) had printed out that ammonia treatment prior to carbon nanotubes growth has been able to break the continuous catalyst film into nano particle islands and reduce oxide layer formed over metal catalyst. The absence of oxide layer and the presence of nano particles reactive lead to reactive carbon atom to dissolve efficiently and precipitated into highly crystalline nanotubes [94].

## 4.4 Transmission Electron Microscopy

Since SEM is unable to observe the inner structure of nanotubes which would be reveal its growth type, further nanotubes structure observation should be carried out by transmission electron microscopy.

## 4.4.1 Catalyst Effect on Carbon Nanotubes Structure

Figure 4-11 and figure 4.12 show carbon nanotubes grown over iron and nickel catalyst film respectively.
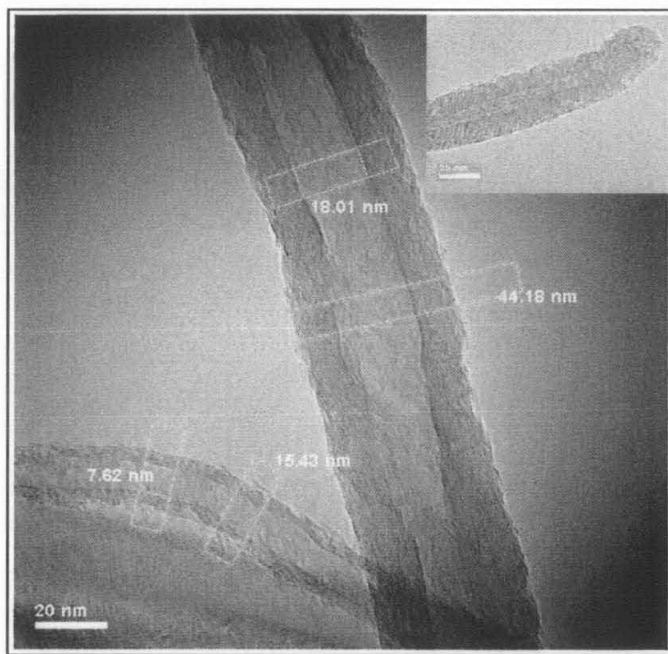
Figure 4-11. TEM image of carbon nanotubes grown over iron catalyst. Inset: carbon nanotubes tips.
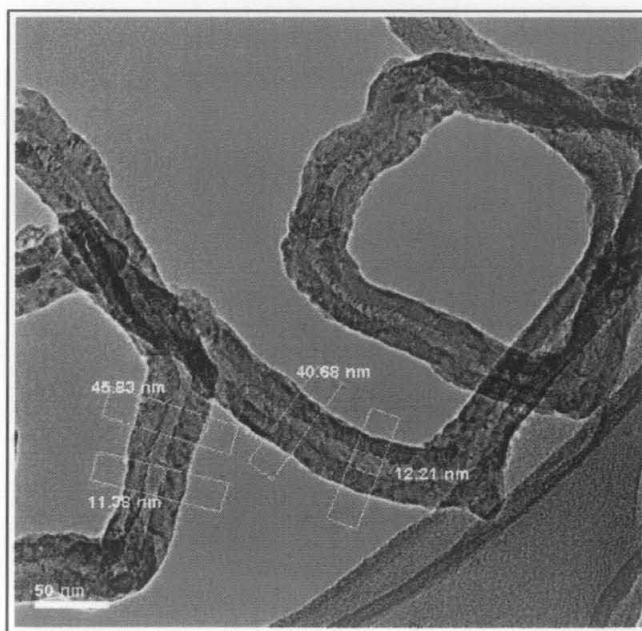


Figure 4-12. TEM image of carbon nanotubes grown over nickel film catalyst.

As shown in the inset of figure 4.11 there is no catalyst particle found at nanotube tip hence it is suggested that carbon nanotubes growth is growth base type. As seen in figure 4.11 and figure 4.12, carbon nanotubes grown over iron catalyst gives better crystallinity than nanotubes grown over nickel catalyst. TEM results agree with Raman spectroscopy analysis which show higher crystallinity obtained from carbon nanotubes grown over iron catalyst. Moreover smaller inner diameter observed in carbon nanotubes grown over iron catalyst is well confirmed with Raman spectroscopy result which shows the presence of RBM peak. Similar observation of better crystallinity with iron catalyst had been reported by Cheol et al (2002) who had use thermal CVD technique [102]. From this result, it is suggested that catalyst affects the nanotubes crystallinity with higher crystallinity is obtained by using iron film catalyst.

## 4.5 Carbon Nanotubes Film Resistivity Measurement

The sheet resistivity of carbon nanotube film from different metal catalyst was examined by using Van der Pauw resistivity measurement technique in four point probe configuration. In this experiment it is found that the sheet resistivity value of carbon nanotubes film grown over iron and nickel catalyst is $51 \times 10^{-4}$ and $75 \times 10^{-4}$ $\Omega cm^{-2}$ respectively. This value is agreeable with the value obtained by using four point probe resistivity technique for well oriented nanotubes ribbon [70]. Singjai et al (2007) suggested that there is a correlation between resistivity and carbon nanotubes crystallinity. Higher nanotubes crystallinity was found to have smaller sheet resistance value [20]. This can be explained by the high mobility electrons in high crystallinity nanotubes since no structural defects obstruct their movement in the nanotubes wall. In addition, on the deformed carbon nanotubes, the chemical bounding of nanotubes in some region had transformed from $sp_2$ to $sp_3$ mode [103]. Since electrical transport on carbon nanotubes is dominated by $sp_2$, the transformation of chemical bounding to $sp_3$ mode would lead to the reduction of nanotubes conductivity.

## 4.6 Hall Effect on Carbon Nanotubes Film

The transport properties of nanotubes film such as carrier type and mobility were examined through Hall Effect measurement using configuration shown in figure 4.13. The obtained result is tabulated in table 4-3.
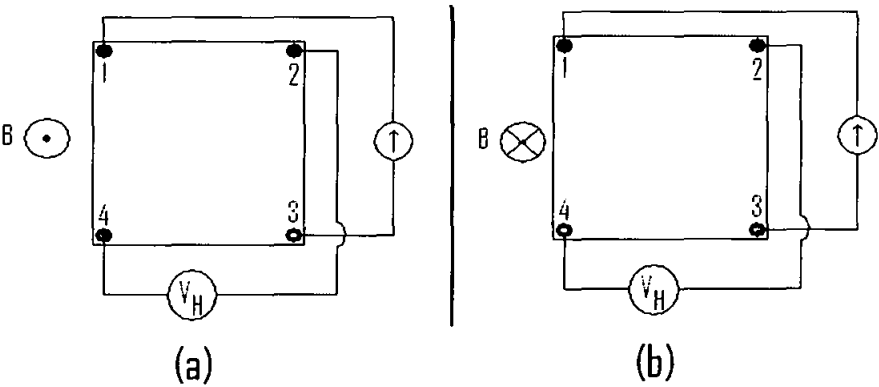


Figure 4-13 Hall effect measurement configuration (a) $V_{xxp}$ measurement

(b) $V_{xxn}$ measurement

Table 4-3 Hall Voltage of Carbon Nanotubes Film

|  | Vc | Vd | Ve | Vf | Hall voltage offset (mV) |
|---|---|---|---|---|---|
| Iron | -0,039 | 0,029 | 0,029 | -0,026 | -0,007 |
| Nickel | -0,007 | -0,003 | -0,008 | 0,009 | -0,009 |

The carrier types in carbon nanotubes film, whether n-type or p-type, are determined from total summation of Hall offset voltage which is shown in equation 4.1.

$$V_c + V_d + V_e + V_f \quad \begin{cases} Total\_Hall\_offset\_Voltage \quad < 0 \quad ; n-type \\ Total\_Hall\_offset\_Voltage \quad > 0 \quad ; p-type \end{cases} \qquad (4.1)$$

Where :   $V_c$   $= V_{24p} - V_{24n}$      $V_d$   $= V_{42p} - V_{42n}$

$V_e$   $= V_{13p} - V_{13n}$      $V_f$   $= V_{31p} - V_{31n}$

As shown in table 4-3, both carbon nanotubes grown on nickel and iron catalysts give negative total offset voltage. Therefore carrier type on carbon nanotubes film is of $n$-type.

Sheet carrier density ($n_s$) of nanotubes film is calculated using equation 4.2

$$\mu = \frac{1}{qR_s n_s}$$ (4.2)

Where:

$$n_s = \left| \frac{8x10^{-8} IB}{q(V_c + V_d + V_e + V_f)} \right|$$ (4.3)

$\mu$ = Hall mobility

q = electrical charge = 1.602 x 10$^{-19}$ Coulomb

I = Current

B= Magnetic field

From equation 4.3, electron mobility of iron and nickel catalyzed MWCNTs are found to be 3.36 x $10^3$ cm$^2$/Vs and 2.94 x $10^3$ cm$^2$/Vs respectively. This result is observed to be lower than vertically aligned MWCNTs film reported by Saravanan (2005) which the value is 14.4 x $10^3$ cm$^2$/Vs [104]. The lower electron mobility on nanotubes film is expected due to by not well oriented nanotubes which hinder electron movement on the film.

## 4.7 Carbon Nanotubes Based Gas Sensor Application

The sensing properties discussion is started by analyzing the breakdown voltage of various gases followed by the effect of interelectrode separation on the gas breakdown voltage. The next following section will discuss the effect of the gas volume content on the testing chamber to the sensing properties of nanotubes. The other output sensing properties discussion namely operating temperature is also included in this chapter.

### 4.7.1 Gases Breakdown Voltage

In order to study the breakdown voltage of various gases, the sensor setup with 80 $\mu$m interelectrode separation was subjected to the 10 mL gas. The result is shown in figure

4.13 and tabulated in table 4-4. Detail measurement of gas breakdown voltage can be found in Appendix B.
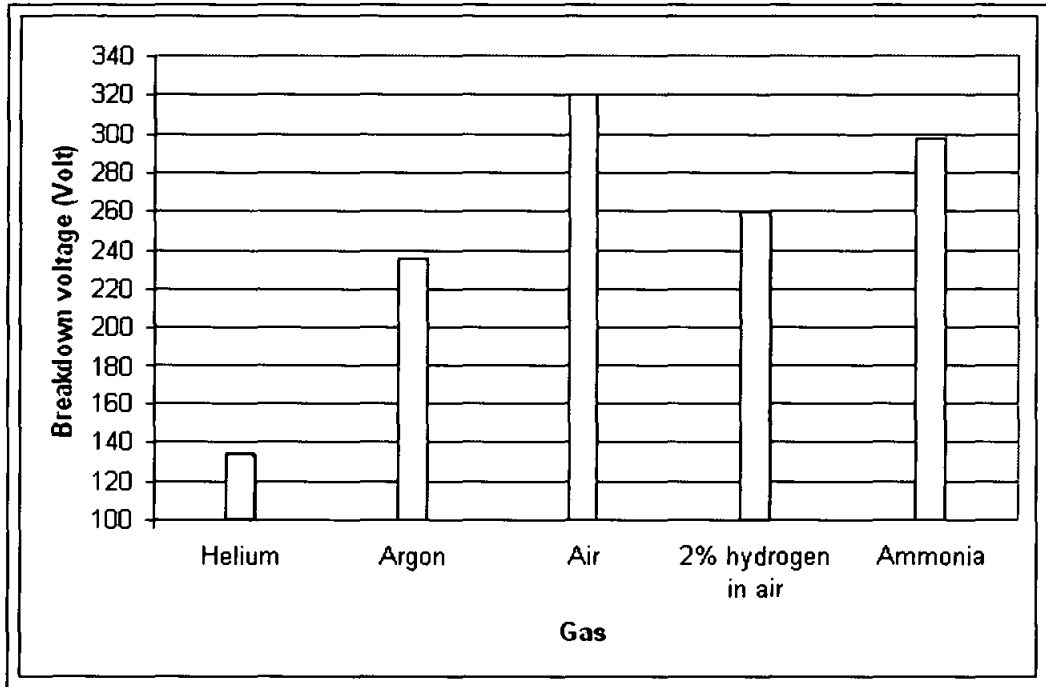


Figure 4-14. Breakdown voltage of 10 mL gas on 80 μm interelectrode separation.

Table 4-4 Gas Breakdown Voltage of Various Gases at 80 μm Interelectrode Separation

| Gas | Breakdown voltage (Volt) |
|---|---|
| Helium | 134 |
| Argon | 236 |
| Air | 320 |
| 2% hydrogen in air | 260 |
| Ammonia | 298 |

Modi et al (2003) found that utilization of aluminum on both anode and cathode film with interelectrode separation of 30 to 160 μm leads to air breakdown voltage of about 350 to 1050 V. Air breakdown voltage was found of about 950 V in 140 μm interelectrode

separation of aluminum anode and cathode [83]. On this work, the same 140 $\mu$m interelectrode configuration with utilization of carbon nanotubes film cathode and aluminum film anode lead to air breakdown voltage of about 440 volt. Hence, the use of carbon nanotubes film had managed to reduce the breakdown voltage by about 58%.

As observed in figure 4.3, helium gives the lowest breakdown value of 134 V whilst the highest value is obtained for air. The breakdown voltage of respective gas can be explained through molecule mean free path approach. The gases mean free path value is ordered from the highest value to lowest as follow: $\lambda_{helium} > \lambda_{hydrogen} > \lambda_{argon} > \lambda_{air} > \lambda_{ammonia}$. Higher mean free path lead to higher energy gained by the electron [105]. Since helium mean free path is the highest among the other gases, electron move due to electric field on helium gas gain the highest energy compare to other gases in the same electric field. Hence, in the same electric field, helium is easier to be ionized by high energy electron collision. Naturally, the breakdown voltage of argon and air will have higher value.

It is obvious in figure 4.13, that 2% hydrogen mixture in air is capable of reducing air breakdown voltage by about 60 V. The reduction in the breakdown voltage is due to prior ionization of hydrogen in air, since hydrogen mean free path is higher than air. Moreover, the reduction of breakdown voltage is attributed to the penning effect on the mixture gas. The effect explains that the lowering of gas breakdown voltage is due to lower ionization energy of one species gas in the gas mixture. Since hydrogen have lower ionization energy compared to other gas components (nitrogen and oxygen) in dry purified air, at the same electric field the ionization of hydrogen molecules occur earlier than nitrogen or oxygen molecules. Hence the 2% mixture hydrogen in air results in lower breakdown voltage compared to breakdown voltage in purified air.

The breakdown voltage of ammonia was found to be lower than air, despite having higher mean free path than air. The reduction of breakdown voltage is attributed to molecule polarization properties of ammonia. Comparing to air, ammonia molecule has dipole moment which leads to molecule polarization. Ionization in polar molecule

requires less energy compared to non polar molecule such as nitrogen and oxygen. Therefore, collisions between ammonia molecules and electron would ionize the gas at lower electric field compared to the air.

As shown in table 4-5, the breakdown voltage difference of each gas to the other is quite prominent. The smallest difference occurs between ammonia and air (22 V) whilst the highest occurs between helium and air (186 V). Although breakdown voltage deviation between ammonia and air quite small, this sensor still can be used to distinguish these gasses. Explanation relating to the effect gas volume content on the breakdown voltage will be discussed in detail in section 4.6.3.

Table 4-5 Difference of Gasses Breakdown Voltage.

| Gas | Helium | Argon | Air | 2% Hydrogen in Air | Ammonia |
|---|---|---|---|---|---|
| Helium | | 102 | 186 | 126 | 164 |
| Argon | | | 84 | 24 | 62 |
| Air | | | | 60 | 22 |
| 2% hydrogen in air | | | | | 38 |
| Ammonia | | | | | |

## 4.7.2   Interelectrode Separation Effect

To study the effect of interelectrode separation on the breakdown voltage, a number of interelectrode separations of nanotubes cathode and aluminum anode are examined. A plot of interelectrode gap to breakdown voltage is shown in figure 4.14 and the values are tabulated in table 4-6.
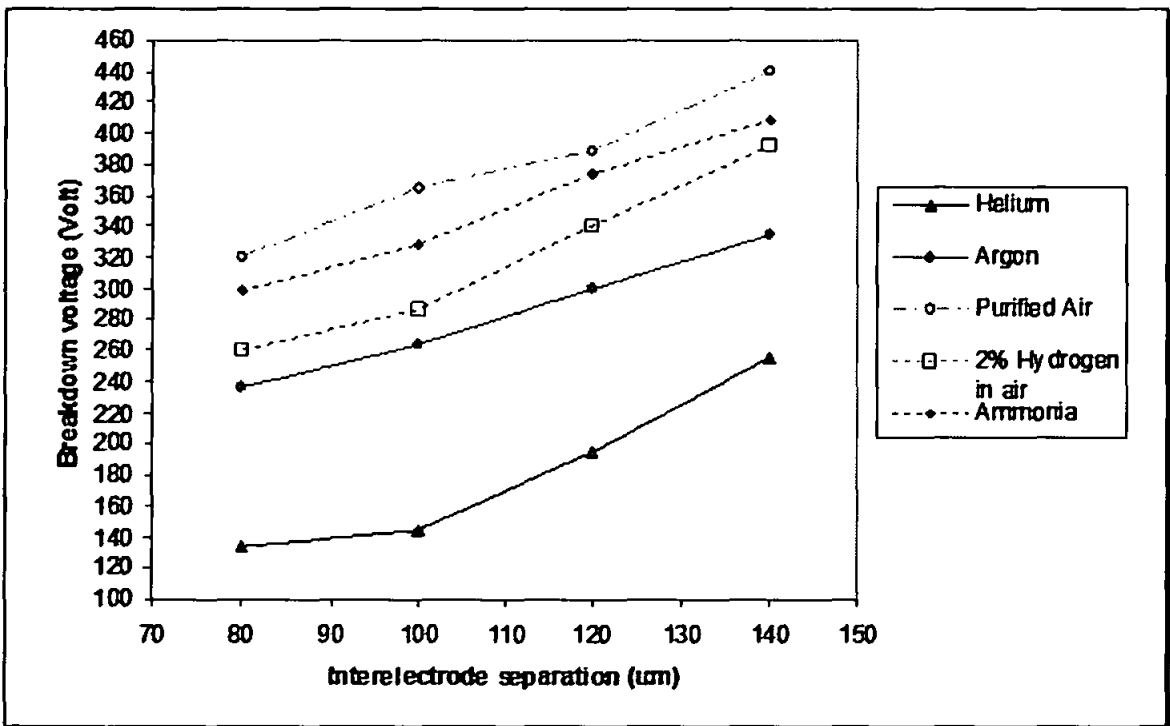
Figure 4-15 Effect of interelectrode separation to breakdown voltage.

Table 4-6 Breakdown Voltage on Various Interelectrode Separation

| Interelectrode separation (mm) | Gas Breakdown Voltage (Volt) | | | | |
|---|---|---|---|---|---|
| | Helium | Argon | Air | 2% Hydrogen in Air | Ammonia |
| 80 | 134 | 236 | 320 | 260 | 298 |
| 100 | 144 | 264 | 364 | 286 | 328 |
| 120 | 194 | 300 | 388 | 340 | 374 |
| 140 | 256 | 335 | 440 | 392 | 408 |

It can be seen from figure 4.14 that the increments in interelectrode separation lead to higher breakdown voltage. Increasing the electrode gap would result in the reduction of electric field between anode and cathode. As the effect, energy gained by the electron from electric field is not sufficient to ionize gas molecule since the electron kinetic energy is lower than gas molecule ionization potential. Hence, for wider interelectrode separation, higher electric field is required to generate gas ionization caused by the collision between electrons and gas molecules.

68

### 4.7.3 Gas Volume Content Effect

The sensitivity of gas sensor to detect the presence of gas is examined by flown in various gases into the vacuum chamber in the different gas volume content. The volume is controlled by gas flowrate outfitted to the chamber. Figure 4-16 shows the testing result of this sensing property whilst the exact values of breakdown voltage of gas sensors are tabulated in table 4-7.
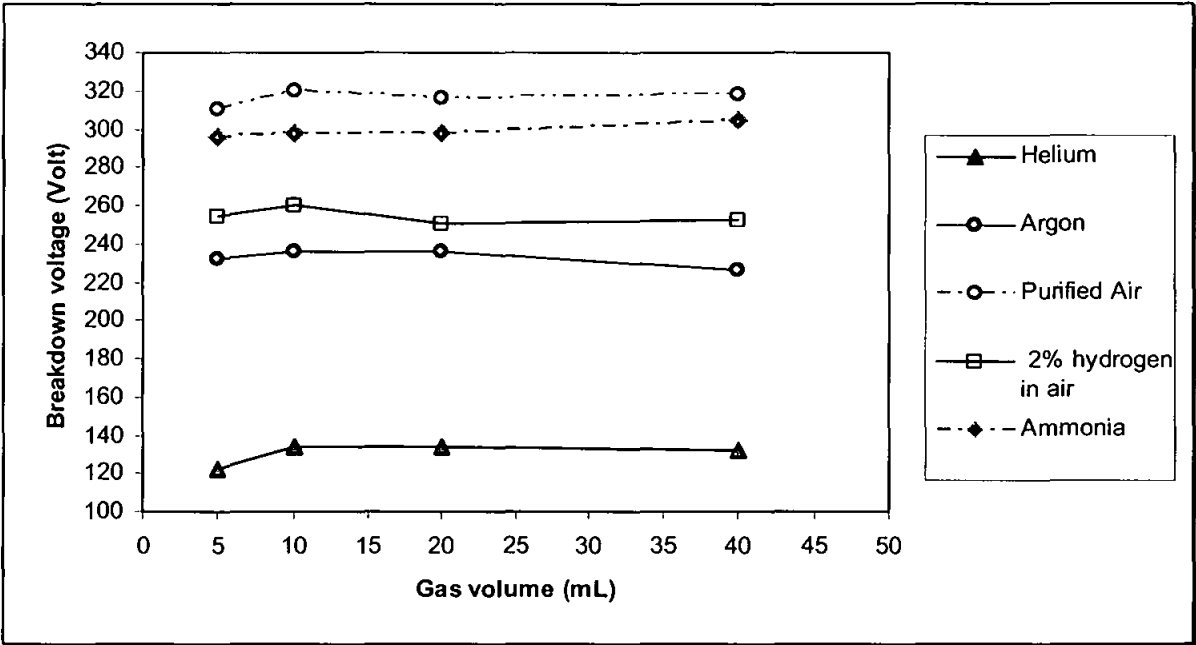


Figure 4-16. Effect of gas volume content to breakdown voltage.

Table 4-7 Breakdown Voltage on Various Gas Volume Content.

| Gas Volume (mL) | Gas Breakdown Voltage (Volt) | | | | |
|---|---|---|---|---|---|
| | Helium | Argon | Air | 2% Hydrogen in Air | Ammonia |
| 5 | 122 | 232 | 310 | 254 | 296 |
| 10 | 134 | 236 | 320 | 260 | 298 |
| 20 | 134 | 236 | 316 | 250 | 298 |
| 40 | 132 | 226 | 318 | 252 | 304 |

It is observed in figure 4.15 that the additional gas volume content does not significantly affect the breakdown voltage of each gas. Modi et al (2003) suggest that the behavior of breakdown over nanotubes and aluminum plate is dominated by highly nonlinear electric field over nanotubes cathode. This phenomenon reduces the sensitivity of the breakdown voltage to the number of the gas molecule [83].

### 4.7.4 Time Lag and Operating Temperature

In this work, transition time from zero current to the appearance of the breakdown voltage is defined as the response time. For accurate measurement, interelectrode voltage increases gradually at about 2 Volt/second. In our experiment it was recorded that the transition time of current happens within a second.

The experiment was carried out at room temperature without applying any heat treatment to the nanotubes film which is used as the active component in the gas sensor setup.

### 4.8 Summary

This work can be classified into three main stages specifically synthesis, characterization, and testing carbon nanotubes as active component on gas sensor. The experiment shows that the oxide layer of silicon substrate influence the carbon nanotubes yield. The yield of carbon nanotubes grown over the oxide layer thickness of about 100 nm is very low and dominated by silicide formation. However, on the oxide layer thickness of about 200 nm high yield carbon nanotubes film is obtained without any silicide formation. The study of catalyst effect to nanotubes structure and electrical properties using Raman spectroscopy shows that carbon nanotubes grown over iron catalyst give better crystallinity compare to nanotubes grown over nickel catalyst. In addition, utilization of iron thin film as the catalyst leads to higher conductivity and mobility nanotubes film compare to utilization of nickel thin film catalyst. The examination of catalyst treatment discloses that the high temperature ammonia atmosphere subjected to iron catalyst coated substrate gives better crystallinity than the one without any catalyst treatment. Testing carbon nanotubes film

as active component in gas sensor reveals that the reduction of interelectrode separation results in the lowering of breakdown voltage. The testing also shows that the breakdown voltage over 5 mL to 40 mL would lead to no significant breakdown voltage variation of tested gases. Breakdown voltage testing over various 10 mL gases on 80 µm interelectrode separation reveals that helium gives the lowest breakdown voltage of 134 V whilst the highest breakdown voltage is obtained for air. The mixture of 2% hydrogen in air is capable of reducing gas breakdown voltage by about 60 V. The gas sensor is also found to operate at room temperature.

# Chapter 5 : Conclusions and Recommendations

## 5.1 Introduction

The conclusion of synthesis, characterization and testing carbon nanotubes film for sensing application is discussed at the beginning of this chapter. The section after conclusion will be recommendation for future work. The benefit of this work will be explained at the end of this chapter.

## 5.2 Conclusions

The development of carbon nanotubes film has been carried out by synthesizing carbon nanotubes and characterizing its properties. The optimum parameter for synthesizing carbon nanotubes film by ethylene decomposition over the metal catalyst using thermal CVD technique had been found. Testing gas breakdown voltage over metal - carbon nanotubes film electrode has been carried out successfully. The testing reveals breakdown voltage over various gases, and also discloses the effect of interelectrode separation and gas volume content to the breakdown voltages

The high yield carbon nanotubes film without any silicide formation is obtained from the decomposition of carbon feedstock on metal catalyst over oxide layer thickness of about 200 nm. Highly crystalline carbon nanotubes are obtained by utilization of iron as catalyst in the nanotubes synthesis. In addition, utilization of iron thin film as catalyst results in higher conductivity and mobility of carbon nanotubes film compared to the one using nickel catalyst. Hollow and less defective site of carbon nanotubes is also obtained from the use of iron catalyst on the nanotubes synthesis. The iron catalyst treatment on

high temperature ammonia atmosphere was found to give high crystalline carbon nanotubes.

The testing of metal - nanotubes film electrodes in room temperature over various gases reveals that the breakdown voltage is unique for every gas. The breakdown voltage of each gas is ordered from the lowest to the highest value as the following order: helium, argon, 2% hydrogen in air, ammonia, and air. The testing also reveals that gas volume content does not affect the gas breakdown voltage. Furthermore, it was shown that the gas breakdown Voltage can be decreased by reducing interelectrode separation. From these results it can be concluded that carbon nanotubes film promising to be used for gas sensing application.

## 5.3 Recommendations

Based on this work, some recommendations for future work that may gives deeper insight into ionization based gas sensor using carbon nanotubes are listed in this section.

At first, further study on the synthesis of vertically aligned carbon nanotubes is highly necessary. The vertically aligned carbon nanotubes as cathode are believed to give lower breakdown voltage since it is expected to give higher electric field in-between the electrodes. In order to obtain the aligned nanotubes, either $Al_2O_3$ [106] or thick $SiO_2$ is suggested to be used as catalyst buffer. Porous $Al_2O_3$ layer suppose to give better support area which is expected to improve the capability of diffusion of atom carbon to metal catalyst hence better alignment nanotubes can be obtained.

Secondly, since the breakdown voltage on mixture gas is affected by its composition, the testing on various concentrations with two or more mixture gas is suggested to be carried out. Hence more gases can be identified using this sensing mechanism.

## 5.4 Benefits

The benefits of ionization mechanism based gas sensing application using multiwalled carbon nanotubes are:

1. The utilization of carbon nanotubes film as cathode is able to reduce breakdown voltage of about 58% compared to aluminum film cathode.

2. The gas breakdown voltage creates finger print that can be used for identifying various gases using single sensor.

3. The ionization mechanism for gas detection capable of operating at room temperature.

4. Due to the design of sensing element is not complicated and easy integration with sensor electrical part, this sensing configuration is promising for low cost production..

# References :

[1]     V. Aroutiounian, "Metal oxide hydrogen, oxygen, and carbon monoxide sensors for hydrogen setups and cells," *International Journal of Hydrogen Energy*, vol. 32, pp. 1145-1158, 2007.

[2]     J. P. V. C. Pijolat, G. Tournier, P. Montmeat, "Application of membranes and filtering films for gas sensors improvements," *Thin Solid Films*, vol. 490, pp. 7-16, 2005.

[3]     J.-M. B. Niels de Jonge, "Carbon Nanotube Electron Sources and Applications," *Phil. Trans. R. Soc. Lond A*, vol. 362, pp. 2239-2266, 2004.

[4]     S. D. S.Ciraci, T Yildirim, O.G ulseren, R.T Senger, "Functionalized carbon nanotubes and device applications," *J. Phys.: Condens. Matter*, vol. 16, pp. R901-R960, 2004.

[5]     G. M. A. Pantano, F. Cappello, "Multiwalled Carbon Nanotube Reinforced Polymer Composites," *Materials Science and Engineering A*, 2007.

[6]     M. Q. Guixin Wang, Zuolong Yu, Rongzhong Yuan, "LiNi0.8Co0.2O2/MWCNT composite electrodes for supercapacitors," *Materials Chemistry and Physics*, vol. 105, pp. 169–174, 2007.

[7]     P. A, "Carbon Nanotubes Resonator Sensors For Remote Sensing Systems," in *IEEE Topical Confrence on Wireless Communication Technology*, 2003.

[8]     S. M. Cho, Young Jun Kim, Yong Shin Kim, Yoonseok Yang, Seung-Chul Ha  " The application of carbon nanotube-polymer composite as gas sensing materials," *Sensors, Proceedings of IEEE*, vol. 2, pp. 701- 704 2004.

[9]     P. D. K. O. K. Varghese, D. Gong, K. G. Ong, E. C. Dickey, C. A. Grimes, "Gas Sensing Characteristic of Multi-Wall Carbon Nanotube," *Sensors and Actuators B*, vol. 81, pp. 32-41, 2001.

[10]    T.-W. C. Chun-Yu Li, "Strain and pressure sensing using single-walled carbon nanotubes," *Nanotechnology*, vol. 15, pp. 1493-1496, 2004.

[11]    J. R. H. H. W. Kroto, S. C. O'Brien, R. F. Curl , R. E. Smalley, "C60:Buckminstefullerene," *Nature*, pp. 162-163, 1985.

[12]    S. Iijima, "Helical Micotubules of Graphitic Carbon," *Nature*, pp. 56-58, 1991.

[13]    Kebes, "CNTnames.png," 2005.

[14]    Arnero, "Carbon nanotube armchair povray.PNG," 2007.

[15]    S. R. Christian Thomsen, Janina Maultzsch, *Carbon Nanotubes*: Wiley-VCH, 2004.

[16]    P. J. F. Harris, *Carbon nanotubes and related Structure new material for the twenty-first century*: Cambridge University Press, 1999.

[17]    C. L. K. Zhen Yao, Cees Dekker, "High-Field Electrical Transport in Single-Wall Carbon Nanotubes," *Physical Review Letters*, vol. 84, Number 13, pp. 2941-2944, 2000.

[18]    J. X. Lingbo Zhu, Yonghao Xiu, Yangyang Sun, Dennis W.Hess, C.P. Wong, "Growth and electrical characterization of high-aspect-ratio carbon nanotube arrays," *Carbon*, vol. 44, pp. 253-258, 2006.

[19]   D. K. L. J.W. Jang, C.E. Lee, T.J. Lee, C.J Lee, S.J Noh, "Metallic Conductivty in Bamboo-shaped multiwalled Carbon nanotubes," *Solid State Communication*, vol. 122, pp. 619-622, 2002.

[20]   S. C. P. Singjai, S. Thongtem, "Electrical Resistivity of bulk multi-walled carbon nanotubes synthesized by an infusion chemical vapor deposition method," *Materials Science and Engineering A*, vol. 443, pp. 42-46, 2007.

[21]   W. D. Gang Zhou, Binglin Gu, "Electronic Structure and Field-Emission Characteristics of Open-Ended Single-Walled Carbon Nanotubes," *Physical Review Letters*, vol. 87 Number 9, pp. 095504-1 - 095504-4, 2001.

[22]   L. W. Zhang Yuning, Zhang Xiaobing, Wang Baoping, "Calculation of the emission performance of the carbon nanotube array," *Applied Surface Science*, vol. 245, pp. 400-406, 2005.

[23]   M. L. L.M. Sheng, P. Liu, Y. Wei, L. Liu, S.S. Fan, "Field emission from self-assembly structure of carbon-nanotube," *Applied Surface Science*, vol. 250, pp. 9-13, 2005.

[24]   C.-C. C. Jyh-Hua Ting, Shaun-Laing Chen, Duan-Shaw Lu, Chung-Yuan Kung , Fuang-Yuan Huang, "Optimization of field emission properties of carbon nanotubes by Taguchi method," *Thin Solid Films*, vol. 496, pp. 299 - 305, 2006.

[25]   T.-W. C. Chunyu Li, "Elastic moduli of multi-walled carbon nanotubes and the effect of van der Waals forces," *Composites Science and Technology*, vol. 63, pp. 1517-1524, 2003.

[26]   O. J. A. Gorbunov, W. Pompea, A. Graffb, "Solid–liquid–solid growth mechanism of single-wall carbon nanotubes," *Carbon*, vol. 40, pp. 113 -118, 2002.

[27]   O. J. A. Gorbunov, W.Pompe, A.Graft, "Role of the catalyst size in the synthesis SWCNTs," *Applied Surface Science*, vol. 197-198, pp. 563-567, 2002.

[28]   R. D. d. F. M. Daenen, B. Hamers, P.G.A. Janssen, K. Schouteden, M.A.J. Veld, "The Wondrous World of Carbon Nanotubes 'a review of current carbon nanotube technologies'," 2003.

[29]   F. D. Xin Lv, Yanfeng Ma, Qiang Wu, Yongsheng Chen, "Synthesis of high quality single-walled carbon nanotubes at large scale by electric arc using metal compounds," *Letters to the Editor / Carbon*, vol. 43, pp. 2013–2032, 2005.

[30]   H. J. K. Hyeon Hwan Kim, "Preparation of carbon nanotubes by DC arc discharge process under reduced pressure in an air atmosphere," *Materials Science and Engineering B*, vol. 133, pp. 241–244, 2006.

[31]   M. H. R. m. Xinhua Lin, Thomas Gemming, Thomas Pichler, Dediu Valentin, Giampiero Ruani, Carlo Taliani, "Single-wall carbon nanotubes prepared with different kinds of Ni–Co catalysts: Raman and optical spectrum analysis," *Article In Press, Carbon*, 2006.

[32]   P. M. A. G. Radhakrishnan, L.S. Bernstein, "Room-temperature deposition of carbon nanomaterials by excimer laser ablation," *Thin Solid Films*, vol. 515, pp. 1142–1146, 2006.

[33]   C. X. H. Griffiths, T. Barrass, M. Cooke, F. Iacopi, P. Vereecken , S. Esconjauregui, "Plasma assisted growth of nanotubes and nanowires," *Surface & Coatings Technology*, vol. 201, pp. 9215–9220, 2007.

[34]    B. W. Tingzhi Wang, "Study on structure change of carbon nanotubes depending on different reaction gases," *Applied Surface Science*, vol. 253, pp. 1606–1610, 2006.

[35]    I. A. Caterina Ducati, Manish Chhowalla, Gehan A. J. Amaratunga, John Robertson, "Temperature selective growth of carbon nanotubes by chemical vapor deposition," *J. Appl. Phys*, vol. 92 no 6, pp. 3299-3303, 2002.

[36]    A. L.-P.-T. P. Finnie , J. Lefebvre , D.G. Austing, "Optimization of methane cold wall chemical vapor deposition for the production of single walled carbon nanotubes and devices," *Carbon, Article In Press,*, 2006.

[37]    H. O. Pierson, *Handbook of chemical vapor deposition*: William Andrew Publishing, 1999.

[38]    H. N. Y. Kobayashia, D. Takagib, Y. Hommaa, "CVD growth of single-walled carbon nanotubes using size-controlled nanoparticle catalyst," *Thin Solid Films*, vol. 464-465, pp. 286-289, 2006.

[39]    A. H. S. Anastasios John Hart, Laure Royer, "Growth of conformal single-walled carbon nanotube films from Mo/Fe/Al2O3 deposited by electron beam evaporation," *Carbon*, vol. 44, pp. 348-359, 2006.

[40]    B. H. Kim Yen Tran, Jean-Francois Colomer, Jean-Paul Pirard,Stephanie Lambert, "Carbon nanotubes synthesis by the ethylene chemical catalytic vapour deposition (CCVD) process on Fe, Co, and Fe-Co/Al2O3 sol-gel catalysts," *Applied Catalysis A, Article In Press,* 2006.

[41]    A. G. N. Paula Queipo, David Gonzalez, Unto Tapper, Hua Jiang Taku Tsuneta, Kestas Grigoras, Jose A. Duen?as, Esko I. Kauppinen, "Novel catalyst particle production method for CVD growth of single- and double-walled carbon nanotubes," *Letters to the Editor / Carbon*, vol. 44, pp. 1581-1616, 2006.

[42]    A. L. D. M. S.A. Moshkalyova, H.R. Guttie?rrezb, M.A. Cottab, J.W. Swart, "Carbon nanotubes growth by chemical vapor deposition using thin film nickel catalyst," *Materials Science and Engineering B*, vol. 112, pp. 147-153, 2004.

[43]    G. C. Huaping Liu, Yong Zhao, Ruiting Zheng, Changlin Liang,Fei Zhao, Tonghe Zhang, "Controlled growth of Fe catalyst film for synthesis of vertically aligned carbon nanotubes by glancing angle deposition," *Surface & Coatings Technology*, vol. 201, pp. 938-942, 2006.

[44]    J. Y. L. a. C. J. L. Yoon huh, "Well-Aligned Carbon Nanotubes Synthesized by Thermal Chemical Vapor Deposition of Acetylene on Cobalt Nanoparticles," *Jpn. J. Appl. Phys*, vol. 42, pp. 7154-7156, 2003.

[45]    E. A. D. V.Z. Mordkovich, A.R. Karaeva, D.N. Kharitonov, I.A. Maslov, A.A. Kamenev, V.F. Tretjakov, "Synthesis of carbon nanotubes by catalytic conversion of methane: Competition between active components of catalyst," *Carbon, Article In Press,*, 2006.

[46]    Y. K. Massimiliano Corrias, Philippe Kalck, Philippe Serp, "CVD from ethylene on cobalt ferrite catalysts: The effect of the support," *Letters to the Editor / Carbon*, vol. 43, pp. 2817-2833, 2005.

[47]    G. E. Y. Y. Wei, V. I. Merkulov, D. H. Lowndes, "Effect of catalyst film thickness on carbon nanotube growth by selective area chemical vapor deposition," *Applied Physics Letters*, vol. 78, pp. 1394-1396, 2004.

[48]   J. C. Zongquan Li, Xixiang Zhang, Yongdan Li, Kwok Kwong Fung, "Catalytic synthesized carbon nanostructures from methane using nanocrystalline Ni," *Carbon*, vol. 40, pp. 409-415, 2002.

[49]   S. H. S. Z. Siang-Piao Chai, Abdul Rahman Mohamed, "Formation of Y-junction carbon nanotubes by catalytic CVD of methane," *Solid State Communications*, vol. 140, pp. 248-250, 2006.

[50]   C.-S. C. Jarrn-Horng Lin, Hui-Ling Ma, Chen-Yin Hsu,Hsiu-Wei Chen, "Synthesis of MWCNTs on CuSO4/Al2O3 using chemical vapor deposition from methane," *Carbon, Article In Press,,* 2006.

[51]   H. R. B.K. Singh, Rajeev C. Chikate, Nguyen Duc Hoac, Soo Jin Park, Seok Kim, Jae Rock Lee, "Growth of multiwalled carbon nanotubes from acetylene over in situ formed Co nanoparticles on MgO support," *Solid State Communications* vol. 139, pp. 102–107, 2006.

[52]   P. S. Roberto Marangonia, Roselyne Feurerb, Yolande Kihnc,Philippe Kalck, Constantin Vahlas, "Carbon nanotubes produced by substrate free metalorganic chemical vapor deposition of iron catalysts and ethylene," *Carbon*, vol. 39, pp. 443–449, 2001.

[53]   G. R.-M. G. Ortega-Cervantez, J. Ortiz-Lo´pez, "Catalytic CVD production of carbon nanotubes using ethanol," *Microelectronics Journal* vol. 36, pp. 495–498, 2005.

[54]   M.-C. B. Marion Wienecke, Klaus Deistung, Petra Fedtke, Erika Borchartd, "MWCNT coatings obtained by thermal CVD using ethanol decomposition," *Carbon*, vol. 44, pp. 718–723, 2006.

[55]   S. C. T. C.H. Li, S.C. Lo, K.F. Chen, Z.Y. Juang, K.C. Leou, C.H. Tsai, "Pressure effect of low-temperature growth of multi-wall carbon nanotubes on Nickel catalyst/barrier-coated glass by thermal-CVD," *Surface & Coatings Technology* vol. 200, pp. 3220–3223, 2006.

[56]   F. C.-N. H. Yih-Ming Shyu, "Low-temperature growth and field emission of aligned carbon nanotubes by chemical vapor deposition," *Materials Chemistry and Physics*, vol. 72, pp. 223–227, 2001.

[57]   T.-Y. T. Chien-Chao Chiu, Nyan-Hwa Tai, Chi-Yong Lee, "Synthesis of ultra long vertically aligned carbon nanotubes using the rapid heating and cooling system in the thermal chemical vapor deposition process," *Surface & Coatings Technology*, vol. 200, pp. 3215 – 3219, 2006.

[58]   S. H. Mirco Cantoro, Simone Pisana, Vittorio Scardaci, Atlus Parvez, Caterina Ducati, Andrea C. Ferrari, Arthur M. Blackburn, Kai-You Wang and John Robertson, "Catalytic Chemical Vapor Deposition of Single-Wall Carbon Nanotubes at Low Temperatures," *Nano Letters* vol. 6, No. 6 pp. 1107-1112, 2006

[59]   K. N. John R. Ferraro, *Introductory Raman Spectroscopy* 2 edition ed: Academic Press, 2002.

[60]   M. Meyyappan, *Carbon Nanotubes: Science and Applications*: CRC July 15, 2004.

[61]   G. D. M.S Dresselhaus, R. Saito, A.Jorio "Raman spectroscopy of Carbon Nanotubes," *Physics Report* vol. 409, pp. 47 - 99, 2005.

[62] R. S. A. Jorio, J. H. Hafner, C. M. Lieber, M. Hunter, T. McClure, G. Dresselhaus, M. S. Dresselhaus, "Structural (n,m) Determination of Isolated Single-Wall Carbon Nanotubes by Resonant Raman Scattering," *Physical Review Letters*, vol. 86, pp. 1118-1121, 2001.

[63] J. C. M. Rao, E. Richter, U. Schlecht, P. C. Eklund, R. C. Haddon, U. D. Venkateswaran, Y.-K. Kwon, and D. Tománek, "Effect of van der Waals Interactions on the Raman Modes in Single Walled Carbon Nanotubes," *Physical Review Letters* vol. 86, Number 17 pp. 3895-3898, 2001.

[64] S. R. J. Maultzsch, and C. Thomsen, "Chirality-selective Raman scattering of the D mode in carbon nanotubes," *Physical Review B*, vol. 64, 2001.

[65] M. A. P. M.S. Dresselhaus, K. Kneipp, S.D.M. Brown, P. Corio, A. Marucci, and G. Dresselhaus, *Science and Application of Nanotubes*. New York: Kluwer Academic / Plenum Publishers, 2000.

[66] L. D. Z. X.Y. Zhang, G.H. Li, L.X. Zhao, "Template synthesis of well-graphitized carbon nanotube arrays," *Materials Science and Engineering A*, vol. 308, pp. 9-12, 2001.

[67] *Encyclopedia of Materials Characterization - Surfaces, Interfaces, Thin Films*: Elsevier, 1992.

[68] Y.-F. C. T. Brintlinger, T. Dü˝rkop, Enrique Cobas, and M. S. Fuhrera, John D. Barry, John Melngailis, "Rapid imaging of nanotubes on insulating substrates," *Applied Physics Letters* vol. 81, Number 13 pp. 2454-2456, 2002.

[69] T. J. S. W.R Runyan, *Semiconductor Measurement & Instrumentation*: McGraw-Hill, 1998.

[70] J. W. Yan-Hui Lia, Xianfeng Zhanga, Cailu Xua, Dehai Wua, Li Lub, Bingqing Wei, "Mechanical and electrical properties of carbonnanotube ribbons," *Chemical Physics Letter*, vol. 365, pp. 95-100, 2002.

[71] L. S. a. D.Walsh, *Electrical Properties of Material*. New York: Oxford University Press, 2004.

[72] Peo, "Hall effect.png," 2005.

[73] D. S. C. W. B. Choi, J. H. Kang, H. Y. Kim, Y. W. Jin, I. T. Han, Y. H. Lee, and N. S. L. J. E. Jung, G. S. Park, J. M. Kim, "Fully sealed, high-brightness carbon-nanotube field-emission display," *Applied Physics Letters* vol. 75, NUMBER 20 1999.

[74] P. S. A. Tae Young Lee, Ji-Beom Yoo, "Fabrication of dye sensitized solar cell using TiO2 coated carbon nanotubes," *Thin Solid Films*, vol. 515, pp. 5131–5135, 2007.

[75] J. L. R.Z. Ma , B.Q. Wei, B. Zhang, C.L. Xu, D.H. Wu, "Study of electrochemical capacitors utilizing carbon nanotube electrodes," *Journal of Power Sources* vol. 84, pp. 126–129, 1999.

[76] T. H. Ph. Avouris, R. Martel, T. Schmidt, H.R. Shea, R.E. Walkup, "Carbon nanotubes: nanomechanics, manipulation, and electronic devices," *Applied Surface Science*, vol. 141, pp. 201–209, 1999.

[77] Q. Z. Jingqi Li, Dajiang Yang, Jingze Tian, "Fabrication of carbon nanotube field effect transistors by AC dielectrophoresis method," *Carbon*, vol. 42, pp. 2263–2267, 2004.

[78]   R. T. L. Roschier, M. Ahlskog, M. Paalanen, P. Hakonen, "Manufacture of single electron transistors using AFM manipulation on multiwalled carbon nanotubes," *Microelectronic Engineering*, vol. 61–62, pp. 687–691, 2002.

[79]   K.-H. L. Jaehyun Chung, Junghoon Lee, "Multi-walled carbon nanotube sensors," presented at The 12th Internalianai Conference on Solid Stale Senson, Actualors and MicrosystemS, Boston, 2003.

[80]   S. N. Saurabh Chopra, Apparao M Rao, "Gas sensing using carbon nanotube-based resonator," *Sensors, 2004. Proceedings of IEEE*, vol. 1, pp. 399 - 402, 2004.

[81]   S.-I. M. Yoon-Taek Jang, Jin-Ho Ahn, Yun-Hi Lee, Byeong-Kwon Ju "A simple approach in fabricating chemical sensor using laterally grown multi-walled carbon nanotubes," *Sensors and Actuators B*, vol. 9, pp. 118–122, 2004.

[82]   H.-F. Y. Yan-Li Liu , Yu Yang, Zhi-Min Liu, Guo-Li Shen, Ru-Qin Yu "Gas sensing properties of tin dioxide coated onto multi-walled carbon nanotubes," *Thin Solid Films*, vol. 497, pp. 355 – 360, 2006.

[83]   N. K. Ashish Modi, eric Lass, Bingqing Wei, Pullicel M Ajayan, "Miniaturized Gas Ionization Sensor Using Carbon Nanotubes," *Nature*, vol. 242, pp. 171-174, 2003.

[84]   L. S. a. D. Walsh, *Electrical Properties of Material*, Seventh ed. New YORK: Oxford University Press, 2004.

[85]   G. G. Raju, *Dielectric in Electric Fields*. New York: Marcel Dekker, Inc, 2003.

[86]   V. K. M.S. Naidu, *High Voltage Engineering*: McGraw-Hill, 1995.

[87]   F. F. E. Mohamed Ali Hassouba, A. Abuwali Garamoon, "Measurements of The Breakdown Potentials For Different Cathode Materials In The Townsend Discharge," *FIZIKA A*, vol. 11, pp. 81-90, 2002.

[88]   W. S. Z. E. Kuffel, J. Kuffel, *High Voltage Engineering : Fundamental*: Butterworth-Heinenmann, 2000.

[89]   A. G. Andreou, "Silicon Oxidation Lecture notes adapted from Microfabrication handout notes by Norman Sheppard," 2000.

[90]   G. D. Ewen Smith, *Modern Raman Spectroscopy: A Practical Approach*: John Wiley and Sons, 2005.

[91]   B. W. Yung Joon Jung, Robert Vajtai, Pulickel M. Ajayan, "Mechanism of Selective Growth of Carbon Nanotubes on SiO2/Si Patterns," *Nano Letters*, vol. Vol 3, no 4, pp. 561-564, 2003.

[92]   F. V. T. de los Arcos, M. G. Garnier, V. Thommen, H.-G. Boyen, P. Oelhafen, "Influence of iron–silicon interaction on the growth of carbon nanotubes produced by chemical vapor deposition," *Applied Physics Letters*, vol. Volume 80, Number 13, pp. 2383-2385, 2002.

[93]   M. C. S. Pisana, A. Parvez, S. Hofmann, A.C. Ferrari, J. Robertson, "The role of precursor gases on the surface restructuring of catalyst films during carbon nanotube growth," *Physica E*, vol. 37, 2007.

[94]   C.-J. C. Jung Inn SOHN, Seonghoon LEE, Tae-Yeon SEONG, "Effects of Fe Film Thickness and Pretreatments on the Growth Behaviours of Carbon Nanotubes on Fe-doped (001) Si Substrates," *J. Appl. Phys*, vol. 41, pp. 4731–4736, 2002.
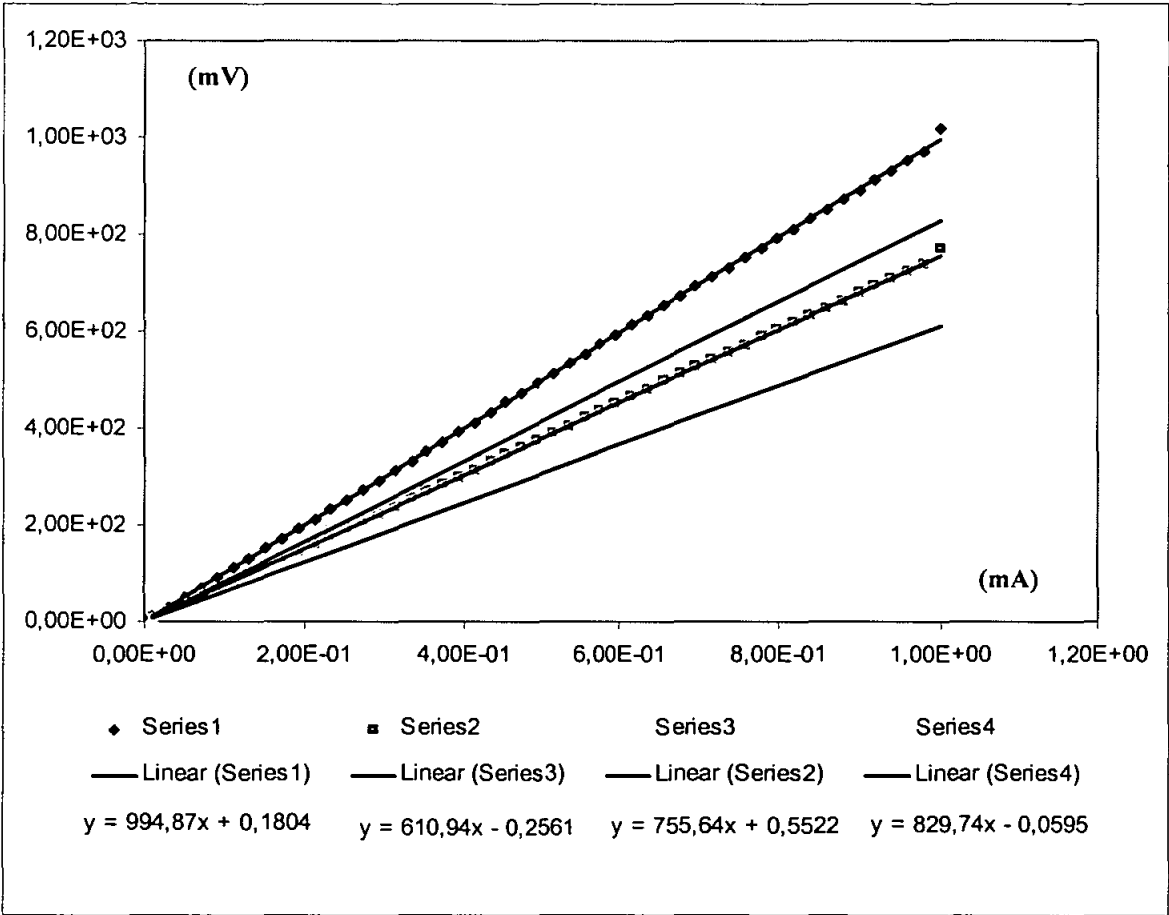
[95] N. Z. Chunnian He, Chunsheng Shi, Xiwen Du, Jiajun Li, "Carbon Nanotubes and Onions from methane decomposition using Ni/Al Catalyst," *Materials Chemistry and Physics*, vol. 97, pp. 109-115, 2006.

[96] G. D. M.S. Dresselhaus, R. Saito, A.Jorio "Raman spectroscopy of Carbon Nanotubes," *Physics Report* vol. 409, pp. 47 - 99, 2005.

[97] Y. C. C. Young Soo Park , Keun Soo Kim , Dong-Chul Chung , Dong Jae Bae , Kay Hyeok An , Seong Chu Lim , Xiao Yan Zhu , Young Hee Lee, "High yield purification of multiwalled carbon nanotubes by selective oxidation during thermal annealing," *Carbon*, vol. 39, pp. 655–661, 2001.

[98] C. Y. C. Chien Chao Chiu, Nyan Hwa Tai, Chuen Horng Tsai, "Growth of high Quality SWNT through Thermal Chemical Vapor Deposition Using co-sputtering Fe-Mo film as Catalysts," *Surface and Coatings Technology*, vol. 200, pp. 3199-3202, 2006.

[99] E. W. Zhenhui Kang, Baodong Mao, Zhongmin Su, Lei Chen, Lin Xu, "Obtaining carbon nanotubes from grass," *Nanotechnology*, vol. 16, pp. 1192–1195, 2005.

[100] J. P. B. J. M. Benoit, O. Chauvet, C. Godon, S. Lefrant, "Low-frequency Raman studies of multiwalled carbon nanotubes: Experiments and theory," *Physical Review B*, vol. 66, 2002.

[101] X. Z. Y. Ando, H. Shimoyama, "Structure analysis of purified multiwalled carbon nanotubes," *Carbon*, vol. 39, pp. 569–574, 2002.

[102] J. P. Cheol Jin Lee, Jeong A. Yu, "Catalyst effect on carbon nanotubes synthesized by thermal chemical vapor deposition," *Chemical Physics Letter*, vol. 360, pp. 250-255, 2002.

[103] A. S. Amitesh Maiti, M. P. Anantram, "Electronic Transport through Carbon Nanotubes: Effects of Structural Deformation and Tube Chirality," *Phys. Review Letter* vol. 88 Number 12, 2002.

[104] S. Muniyandy, "Structural and Electrical Characterization of Aligned Carbon Nanotubes for Gas Sensing Application," in *Electrical and Electronics Engineering*. Tronoh: Universiti Teknologi Petronas, 2005, pp. 109.

[105] G. G. Raju, *Gaseous Electronics Theory and Practice*: CRC Press Taylor & Francis 2006.

[106] N. M. M. M.K.lai, K.M.Begam, "The Role of Al2O3 Buffer Layer in the growth of Aligned CNTs," *Advanced Materials Research*, vol. 32, pp. 29-32, 2008.

# Publications:

1. Hendrayana Thaha, Norani Muti Mohamed, *Synthesis and Characterization of Aligned Single Walled Carbon Nanotubes (SWNTs) for Sensing Application.* Presented at the International Conference on Advancement of Materials and Nanotechnology 2007 (ICAMN 2007), 29$^{th}$ May – 1$^{st}$ June, 2007, Langkawi Island, Malaysia

2. M. Norani Muti, H. Taha, J. S. Lim, M.S. Balbir Singh, *Growth of Aligned Carbon Nanotubes (CNTs) for Application as Functional Devices*, Proceeding of Materials Today Asia Conference 2007, Beijing, China, Sep.2007.

3. M. Norani Muti, H. Thaha, A. Dzilal, J.O. Dennis, *Nanotube-based Chemical Sensors*, Presented at the International Conference on Intelligent and Advanced System, Nov. 2007.

4. M. Norani Muti, H. Thaha, A Dzilal, and J. A. Dennis, *Development of Nanotubes for Gas Sensing Applications*, Presented at the national Physics Conference 2007, Kuala Trengganu,

5. N.M. Mohamed, H. Thaha, *Carbon Nanotubes Gas Sensor*, Accepted for presentation at UK-Malaysia Engineering Conference 2008, 14 -15$^{th}$ July 2008.

6. Hendrayana Thaha, Norani Muti Mohammed, *Study of Sensing Mechanism Using Carbon Nanotubes Film*, Accepted for presentation at international conference on functional materials and devices, 16 -19$^{th}$ June 2008.

# Appendix A: Van der Pauw Sheet Resistance Measurement

First Run [Sample subjected to Positive Voltage]



$y = 994,87x + 0,1804$     $y = 610,94x - 0,2561$     $y = 755,64x + 0,5522$     $y = 829,74x - 0,0595$

First Run [Sample subjected to Negative Voltage]



Series1   Series2   Series3   Series4

—— Linear (Series1) —— Linear (Series2) —— Linear (Series3) —— Linear (Series4)

y = 990,3x - 0,3342   y = 759,13x - 0,0375   y = 609,23x + 0,1827   y = 830,68x + 0,1678

Second Run [Sample subjected to Positive Voltage]



1,20E+03

(mV)

1,00E+03

8,00E+02

6,00E+02

4,00E+02

2,00E+02

0,00E+00

(mA)

0,00E+00   2,00E-01   4,00E-01   6,00E-01   8,00E-01   1,00E+00   1,20E+00

| ◆ Series1 | ◘ Series2 | Series3 | Series4 |
|---|---|---|---|
| ——Linear (Series1) | ——Linear (Series2) | ——Linear (Series4) | ——Linear (Series3) |
| y = 992,12x + 0,566 | y = 755,5x + 0,6281 | y = 610,2x - 0,2538 | y = 829,18x - 0,0542 |

Second Run [Sample subjected to Negative Voltage]



| | | | |
|---|---|---|---|
| ◆ Series1 | ◘ Series2 | Series3 | Series4 (mV) |
| ——Linear (Series1) | ——Linear (Series4) | ——Linear (Series2) | ——Linear (Series3) |
| y = 988,06x - 0,4167 | y = 758,28x - 0,423 | y = 608,54x + 0,1926 | y = 830,36x + 0,2206 |

# Appendix B: Gas Breakdown Voltage

| Gas | Gap Distance (µm) | Gas Volume (mL) | Breakdown voltage (Volt) |
|---|---|---|---|
| Helium | 80 | 5 | 122 |
| | 80 | 10 | 134 |
| | 80 | 20 | 134 |
| | 80 | 40 | 132 |
| | **Gap Distance (µm)** | **Gas Volume (mL)** | **Breakdown voltage (Volt)** |
| | 80 | 10 | 134 |
| | 100 | 10 | 144 |
| | 120 | 10 | 194 |
| | 140 | 10 | 256 |
| **Gas** | **Gap Distance (µm)** | **Gas Volume (mL)** | **Breakdown voltage (Volt)** |
| Argon | 80 | 5 | 232 |
| | 80 | 10 | 236 |
| | 80 | 20 | 236 |
| | 80 | 40 | 226 |
| | **Gap Distance (µm)** | **Gas Volume (mL)** | **Breakdown voltage (Volt)** |
| | 80 | 10 | 236 |
| | 100 | 10 | 264 |
| | 120 | 10 | 300 |
| | 140 | 10 | 335 |
| **Gas** | **Gap Distance (µm)** | **Gas Volume (mL)** | **Breakdown voltage (Volt)** |
| Air | 80 | 5 | 310 |
| | 80 | 10 | 320 |
| | 80 | 20 | 316 |
| | 80 | 40 | 318 |
| | **Gap Distance (µm)** | **Gas Volume (mL)** | **Breakdown voltage (Volt)** |
| | 80 | 10 | 320 |
| | 100 | 10 | 364 |
| | 120 | 10 | 388 |
| | 140 | 10 | 440 |
| **Gas** | **Gap Distance (µm)** | **Gas Volume (mL)** | **Breakdown voltage (Volt)** |
| Hydrogen | 80 | 5 | 254 |
| | 80 | 10 | 260 |
| | 80 | 20 | 250 |
| | 80 | 40 | 252 |
| | **Gap Distance (µm)** | **Gas Volume (mL)** | **Breakdown voltage (Volt)** |
| | 80 | 10 | 260 |
| | 100 | 10 | 286 |
| | 120 | 10 | 340 |
| | 140 | 10 | 392 |

| Gas | Gap Distance | Gas Volume (mL) | Breakdown voltage (Volt) |
|---|---|---|---|
| Ammonia | 80 | 5 | 296 |
| | 80 | 10 | 298 |
| | 80 | 20 | 298 |
| | 80 | 40 | 304 |
| | Gap Distance | Gas Volume (mL) | Breakdown voltage (Volt) |
| | 80 | 10 | 298 |
| | 100 | 10 | 328 |
| | 120 | 10 | 374 |
| | 140 | 10 | 408 |

# Appendix C: EDX Result